cardiomyopathy with conduction defects, but joint contracture is not prominent. The onset of these diseases is usually 2 years or later. Recently, *LMNA*-related congenital muscular dystrophy (L-CMD) was reported as a novel and severe form of laminopathy [2]. L-CMD has variable severity and can be divided in two main groups: a severe group with absent motor development and patients with dropped-head syndrome.

We recently came across an infantile-onset laminopathy patient with marked mononuclear cell infiltrations in his muscle mimicking inflammatory myopathy (Patient 1 in Table 1, Fig. 1A). This patient showed hypotonia and delayed motor milestones with elevation of serum CK levels from 3 months of age. Although, he became ambulant at 15 months of age, he presented proximal dominant muscle weakness and atrophy with no dropped-head at 2 years of age. Corticosteroid therapy was started based on the muscle pathological findings that had beneficial effects on his motor development. *LMNA* gene analysis was done at 6 years of age when his ankle and elbow joint contractures appeared and a heterozygous p.Glu358Lys mutation was identified.

From this result, we screened *LMNA* mutation in the 20 patients with the onset at 2 years or younger who were pathologically suspected as inflammatory myopathy.

2. Patients and methods

2.1. Patients

All clinical materials used in this study were obtained for diagnostic purposes and written informed consent was obtained from guardians of all patients. This work was approved by the Ethical Committee of National Center of Neurology and Psychiatry (NCNP). We retrospectively recruited patients with onset at 2 years or younger who were pathologically suspected to have inflammatory myopathy from a total of 10,874 muscle biopsies stored in the

Table 1
Clinical, radiological, and genetic findings of patients with *LMNA* mutations and inflammatory changes.

Patient #/gender/ *LMNA* mutations	Age at onset /age at biopsy/ age at last consultation	Initial signs/ CK at biopsy	Muscle pathology	Steroid treatment: responsiveness/ age at start of administration/ duration of administration	Age at acquired ambulation/ maximum motor ability	Cardiac involvement	Joint contracture	Respiratory dysfunction	CT/MRI (age)/imaging at thigh	CT/MRI (age)/imaging at calf
1/M/E358K*	3 m/2 y/11 y	Motor delay/900	IC: marked, diffuse; NR: moderate; Fib: mild	Effective/2 y/9 y	15 m/Ambulant	No	6 y: Ankles, elbows, 8 y: rigid spine	No	MRI (8 y)/ selective involvement of VL, VI, VM	MRI (8 y)/ selective involvement of SO, mGC
2/M/R249W*	10 m/10 m/12 y (Died by respiratory failure)	Motor delay/1000	IC: marked, pathy; NR: mild; Fib: mild	Effective/10 m/11 y	Unknown/ambulant	9 y: Heart failure	4 y: Ankles, knees	9 y: Nocturnal NPPV	ND	ND
3/M/N39D	11 m/1 y/16 y	Motor delay/1100	IC: marked, pathy; NR: marked; Fib: mild	Effective/1 y/15 y	18 m/Ambulant	13 y: 200B0 A–V block, 15 y 3° A–V block, pacemaker implantation	1 y: Ankles, knees, hips, Rigid spine from childhood	No	CT (13 y)/DI with relative sparing of RF, GR, SA	CT (13 y)/DI
4/F/R249Q*	2 y/2 y/15 y	High CK/2000	IC: moderate, focal; NR: moderate; Fib: moderate	Effective/3 y/6 m	14 m/Ambulant	12 y: 1° A–V block	3 y: Ankles, 8 y: elbows	No	CT (6 y)/DI with relative sparing of RF, GR	CT (6 y)/ selective involvement of SO, mGC
5/M/R28Q	5 m/1 y/11 y	Motor delay/800	IC: marked, pathy; NR: moderate; Fib: moderate	Ineffective/1 y/2 y	18 m/9 y: Inability to walk	Atrial fibrillation, A–V block, PAC, PVC	No	No	CT (11 y)/DI with relative sparing of RF, GR, SA	ND
6/M/R41S	9 m/1 y/13 y	Motor delay/900	IC: moderate, diffuse, NR: moderate Fib: moderate	Ineffective/1 y/8 y	16 m/9 y: Inability to walk	11 y: PSVT attack	6 y: Ankles, elbows	11 y: Nocturnal NPPV	MRI (10 y)/ DI/DI	MRI (10 y)/ DI/DI
7/F/K32del*	1 y/2 y/6 y	Unsteady gait/800	IC: mild, focal; NR: mild; Fib: mild	Ineffective/2 y/8 m	15 m/5 y: Inability to walk	No	2 y: Ankles	No	CT (4 y)/DI with relative sparing of RF, GR/Selective involvement of SO, mGC	CT (4 y)/DI with relative sparing of RF, GR/Selective involvement of SO, mGC
8/M/R249W*	11 m/1 y/24 y (Died by arrhythmia)	Motor delay/600	IC: marked, pathy; NR: mild; Fib: moderate	Ineffective/1 y/unknown	2 y/12 y: Inability to walk	17 y: 2° A–V block, 23 y complete A–V block	17 y: Ankles, knees	No	ND	ND
9/F/L292P	1 y/8 y/10 y	Motor delay/300	IC: mild, focal; NR: moderate; Fib: marked	Unadministered	16 m/4 y: Inability to walk	6 y: LV dysfunction, 8 y: PAC, PVC	No	No	MRI (8 y)/DI with relative sparing of RF, GR, SA	MRI (8 y)/DI
10/F/R377C*	2 y/4 y/7 y (Died by heart failure)	Unsteady gait/1000	IC: moderate, focal; NR: moderate; Fib: moderate	Unadministered	10 m/ambulant	7 y: DCM (EF:32%)	5 y: Ankles	No	ND	ND
11/F/N456H	2 y/5 y/10 y	Unsteady gait/3000	IC: moderate, focal; NR: moderate; Fib: marked	Unadministered	12 m/ambulant	No	6 y: Ankle, knee, neck, 8 y: rigid spine	No	MRI (10 y)/ DI with relative sparing of RF, GR, SA	MRI (10 y)/ DI

A–V block = atrioventricular conduction block, CK = creatine kinase, CT = computed tomography, DI = diffuse involvement, EF = ejection fraction, Fib = endomysial fibrosis, GR = gracilis, IC = inflammatory cellular infiltration, LV = left ventricle, mGC = medial head of gastrocnemius, MRI = magnetic resonance imaging, NPPV = noninvasive positive-pressure ventilation, NR = necrotic and regenerating process, PAC = premature atrial contraction, PSVT = paroxysmal supraventricular tachycardia, PVC = premature ventricular contraction, RF = rectus femoris, SA = Sartorius, SO = soleus, VI = vastus intermedius, VL = vastus lateralis, VM = vastus medialis.

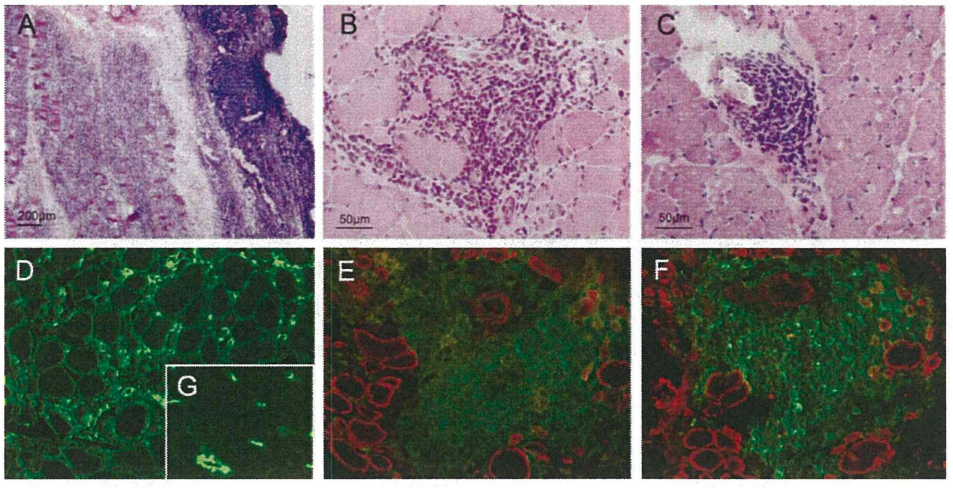

Fig. 1. Inflammatory cellular infiltration observed in the patients with *LMNA* mutations on hematoxilin and eosin staining (A: Patient 1, B: Patient 3, C: Patient 9). Serial frozen sections of muscle from Patient 5 were immunostained with HLA-ABC (D), double immunostained with CD4 (green) and dystrophin (red) (E), and CD20 (green) and dysrophin (red) (F). HLA-ABC stain in control muscle is shown in (G).

National Center of Neurology and Psychiatry. The diagnosis of inflammatory myopathy was based upon the mononuclear cell infiltrations at perimysial, endomysial, and perivascular sites [3]. Patients suspected to have dermatomyositis with skin rash and/or perifascicular atrophy on muscle pathology were excluded in this study. Then we gathered a total of 20 patients including one patient (Patient 2) who had previously been reported as infantile polymyositis [4].

2.2. Histopathological studies

All biopsied samples were taken from biceps brachii. Muscle specimens were frozen in isopentane chilled in liquid nitrogen. Serial frozen sections were stained with hematoxylin and eosin, modified Gomori trichrome, and a battery of histochemical methods. Immunohistochemical analysis was performed as described previously [5]. Antibodies used in this study are: dystrophin (DMDP-II [6], DYS1, DYS2, and DYS3 from Novocastra, Newcastle upon Tyne, UK); sarcoglycans (SGCA, SGCB, SGCG, and SGCD: Novocastra); laminin-α2 chain (ALEXIS, Farmingdale, NY); α-dystroglycan (Upstate Biotech, Lake Placid, NY); caveolin-3 (BD Transduction Laboratories, Franklin Lakes, NJ); dysferlin (Novocastra); emerin (Novocastra); collagen VI (Novocastra); CD4 and CD8 (Nichirei, Tokyo, Japan); CD20, and HLA-ABC (DAKO, Glostrup, Denmark).

2.3. Mutational analysis of LMNA

Genomic DNA was extracted from either frozen muscles or peripheral lymphocytes using standard protocols [7]. All exons and their flanking intronic regions of *LMNA* were amplified by PCR and directly sequenced using automated 3130 sequencer (PE Applied Biosystem, Foster City, CA). Primer sequences are available upon request.

2.4. Clinical information

Clinical characteristics collected from attending physicians were demographic data, age of onset, initial signs, motor functions, presence of cardiac involvement, presence of joint contractures, respiratory function, effectiveness of steroid, and pertinent laboratory examinations including serum creatine kinase (CK), electrocardiogram, Holter electrocardiogram, and echocardiogram.

2.5. Muscle imaging

Muscle computed tomography (CT) or magnetic resonance imaging (MRI) was done with some modifications depending on the facilities in each hospital. Scans were performed at thigh (the largest diameter of thigh) and calf (the largest diameter of lower leg) levels. Involvement of each muscle was evaluated at both scan levels.

3. Results

Ten types of heterozygous single nucleotide substitutions in *LMNA* were identified in 11 of 20 patients. Four (p.Arg249Gln, p.Leu292Pro, p.Asn456His and p.Arg377Cys) mutations were previously reported in patients with AD-EDMD or LGMD1B, one (p.Arg249Trp) was found only in L-CMD patients, and two (p.Lys32del and p.Glu358Lys) were identified in AD-EDMD, LGMD1B, or L-CMD patients [2,8–10]. Another three (p.Arg28Gln, p.Asn39Asp, p.Arg41Ser,) were novel mutations and not detected in 300 control chromosomes. All 11 patients had neither consanguinity nor family history of myopathy or

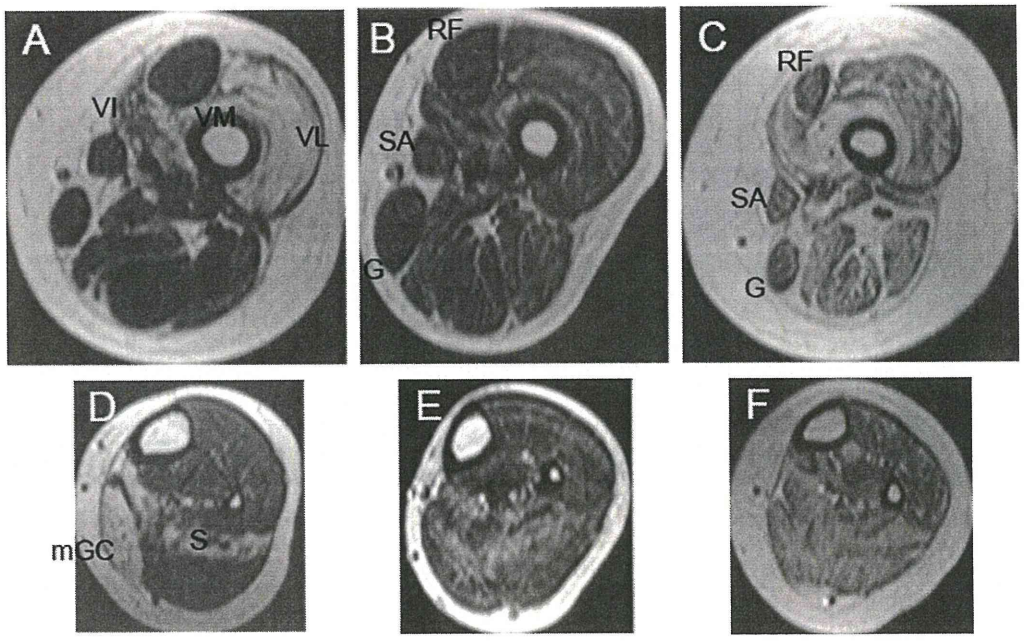

Fig. 2. Selective muscle involvement of thigh and calf muscles. Transverse sections of T1 weighted magnetic resonance imaging of thigh (A–C) and calf (D–F) in patients with *LMNA* mutations. Selective involvements of vastus lateralis (VL), vastus intermedius (VI), vastus medialis (VM), soleus (S), and medial head of gastrocnemius (mGC, A, D: Patient 1), relatively mild and diffuse involvements with relative sparing of rectus femoris (RF), gracilis (G), sartorius (SA, B, E: patient 11), and diffuse and severe involvement with relative sparing of rectus femoris, gracilis, sartorius (C, F: patient 9) are observed.

cardiomyopathy. DNA samples from the parents of 11 patients were not available.

Table 1 shows clinical summary of the 11 patients with *LMNA* mutations. Initial clinical signs were motor developmental delay or progressive muscle weakness. Head drop was not observed in any patient. Serum CK levels were mildly to moderately elevated in all patients. Joint contractures, spinal rigidity, and cardiac involvement were not observed at the time of the biopsy but became prominent in some patients in later age. Importantly, Patient 6 had an episodic paroxysmal supraventricular tachycardia during general anesthesia at age 11 years, and Patient 3 received pacemaker implantation due to complete atrioventricular conduction block at age 15 years. Patient 8 succumbed to sudden death due to arrhythmia at age 24 years and Patient 10 died by cardiac failure at age 7 years. Two patients developed chronic respiratory failure requiring non-invasive positive-pressure ventilation. Patient 2 died by respiratory failure at age 12 years. Steroid was used in eight patients but beneficial effects such as improvement of muscle power and reduction of serum CK levels were seen only in four.

On muscle biopsy, the most striking inflammatory change was observed in Patient 1 showing numerous inflammatory cells predominantly located in the perimysial connective tissue (Fig. 1A). This finding was diffusely seen in the whole muscle specimen. The other 10 patients also showed variable degrees of mononuclear cellular infiltration with active necrosis and regenerating process (Fig. 1B, C, Table 1). Fiber size variation and endomysial fibrosis were also seen. Fiber type grouping, groups of atrophic fibers, and abnormal oxidative stains were not observed. Immunohistochemically, sarcolemmal HLA staining was increased in many fibers in all patients examined (Fig. 1D). Infiltrated mononuclear cells were positive for lymphocyte markers of CD4 (Fig. 1E), CD8 (data not shown), or CD20 (Fig. 1F). No abnormal immunostaining was seen for the antibodies associated with muscular dystrophy (data not shown).

Muscle imaging was performed in relatively later stages of the disease in eight out of 11 patients with *LMNA* mutations (Fig. 2). At the level of thigh, Patient 1 showed selective involvement of vastus lateralis, vastus intermedius and vastus medialis. Patient 6 showed diffuse involvement of all thigh muscles. The remaining six patients showed diffuse involvement of thigh muscles with relative sparing of sartorius, gracilis and rectus femoris. At lower leg levels, three patients (Patients 1, 4, and 7) showed selective involvement of soleus and medial head of gastrocnemius. The remaining four patients showed diffuse involvement of calf muscles.

4. Discussion

In our series, surprisingly, more than half of the infantile patients showing inflammatory changes are due to *LMNA* mutations. Prominent mononuclear cell infiltrations can sometimes be evident in biopsies from muscular dystrophy patients including CMD, LGMD, and facioscapulohumeral muscular dystrophy, leading to misdiagnosis of inflammatory myopathy [11–16]. Apparently, however, frequency of inflammatory changes is much higher in infantile striated muscle laminopathy patients, suggesting a possibil-

ity that *LMNA* mutations may cause active inflammation in skeletal muscle during infancy by a certain mechanism. In support of this notion, three of 15 L-CMD patients report by Quijano-Roy et al. had inflammatory cell infiltration [2]. In Patients 4, 7, 9, 10 and 11, muscle biopsies were done at the age of 2 years or later and inflammatory changes were relatively milder compared to the other earlier biopsies. These findings suggest that severities of inflammation may be related to the age of biopsies.

Inflammatory myopathy manifesting with muscle weakness starting during infancy is a poorly defined muscle disorder and limited number of patients were described in the literature [4,17–20]. Thompson emphasized that responsiveness to corticosteroid is one of the crucial findings that define the infantile myositis [17]. However, this is unlikely to be always the case as some of our laminopathy patients, who were initially diagnosed as infantile-onset inflammatory myopathy also showed some clinical improvement by corticosteroid therapy. Good response to steroids is not only a feature of myositis but can also be seen in other muscular dystrophies including Duchenne muscular dystrophy. Therefore, the possibility of laminopathy should not be excluded solely based upon steroid responsiveness. Interestingly, all steroid-responsive patients were ambulant whereas non-responsive patients could not walk, which might imply some genotype–phenotype correlation. Nonetheless, the correlation between genotype and steroid responsiveness cannot be discussed at this moment as all patients for whom steroid was used had distinct mutations. In any case, corticosteroid therapy could be considered for infantile striated muscle laminopathy patients as some patients respond, although its long-term efficacy is still unknown.

The p.Arg249Trp mutation found in this study was previously reported in L-CMD patients [2], but not in AD-EDMD or LGMD1B. In contrast, p.Glu358Lys mutation has also been reported with extremely variability of phenotypes, including AD-EDMD, LGMD1B, or L-CMD [10]. Thus, the same mutation can result in different phenotypes and severities. These findings raise a possibility that other unknown factor(s) may play a role in the development of laminopathy phenotype.

Muscle imaging demonstrated selective muscle involvement in all eight patients examined. Vastus lateralis and intermedius were markedly affected, while involvement of adductor magnus was minimal. In addition, medial head of the gastrocnemius was remarkably involved while lateral head was relatively spared in most patients. This selective muscle involvement is basically identical to that observed in AD-EDMD/LGMD1B patients [21] and may be helpful for the diagnosis of laminopathy in children.

Cardiomyopathy with conduction defects is a common serious clinical problem in patients with EDMD and LGMD1B [1]. In the present study, 8 of 11 patients developed cardiac complications such as arrhythmia and heart failure in their childhood and two died due to arrhythmia and heart failure, respectively. These findings clearly demonstrate that accurate diagnosis followed by periodic examination of cardiac function including electrocardiogram, holter electrocardiogram and echocardiogram, and appropriate implantation of defibrillators is necessary to avoid unexpected sudden death [22,23].

Our results expand clinical and pathological variation of striated muscle laminopathy and the inflammatory histology is an important diagnostic clue to the *LMNA* related myopathy patients. Further analysis is needed to elucidate the role of mutant A-type lamins in inducing inflammatory process during infancy.

Acknowledgements

We thank Ms. K. Goto and Ms. M. Ohnishi (National Institute of Neuroscience, NCNP) for technical assistance and Dr. M.C.V. Malicdan (National Institute of Neuroscience, NCNP) for reviewing the manuscript. This study was supported by: KAKENHI (21591104) from Japan Society for the Promotion of Science; by Research on Psychiatric and Neurological Diseases and Mental Health of Health Labour Sciences Research Grant and the Research Grant (20B-12, 20B-13) for Nervous and Mental Disorders from the Ministry of Health, Labour, and Welfare; by Research on Health Sciences focusing on Drug Innovation from the Japanese Health Sciences Foundation; and by the Program for Promotion of Fundamental Studies in Health Sciences of the National Institute of Biomedical Innovation (NIBIO).

References

[1] Maraldi NM, Merlini L. Emery–Dreifuss muscular dystrophy. In: Engel AG, Franzini-Armstrong C, editors. Myology. New York, NY: McGraw-Hill; 2004. p. 1027–37.

[2] Quijano-Roy S, Mbieleu B, Bönnemann CG, et al. De novo *LMNA* mutations cause a new form of congenital muscular dystrophy. Ann Neurol 2008;64:81–6.

[3] Gultekin SH. The role of muscle biopsy in the diagnosis of inflammatory myopathy. In: Kagen LJ, editor. The Inflammatory Myopathies. New York, NY: Human Press; 2009. p. 15–28.

[4] Nagai T, Hasegawa T, Saito M, Hayashi S, Nonaka I. Infantile polymyositis: a case report. Brain Dev 1992;14:167–9.

[5] Ishikawa H, Sugie K, Murayama K, et al. Ullrich disease: collagen VI deficiency: EM suggests a new basis for muscular weakness. Neurology 2002;59:920–3.

[6] Arahata K, Hoffman EP, Kunkel LM, et al. Dystrophin diagnosis: comparison of dystrophin abnormalities by immunofluorescence and immunoblot analyses. Proc Natl Acad Sci USA 1989;86:7154–8.

[7] Sambrook J, Russell DW. Molecular Cloning: A Laboratory Manual. Cold Spring Harbor, NY: Cold Spring Harbor Laboratory; 2001.

[8] Park YE, Hayashi YK, Goto K, et al. Nuclear changes in skeletal muscle extend to satellite cells in autosomal dominant Emery–Dreifuss muscular dystrophy/limb girdle muscular dystrophy type 1B. Neuromuscul Disord 2009;19:29–36.

[9] Astejada MN, Goto K, Nagano A, et al. Emerinopathy and laminopathy clinical, pathological and molecular features of muscular dystrophy with nuclear envelopathy in Japan. Acta Myol 2007;26:159–64.

[10] Mercuri E, Poppe M, Quinllvan R, et al. Extreme variability of phenotype in patients with an identical missense mutation in the *lamin* A/C gene: from congenital onset with severe phenotype to milder classic Emery–Dreifuss variant. Arch Neurol 2004;61:690–4.

[11] Amato AA, Griggs RC. Unicorns, dragons, polymyositis, and other mythological beasts. Neurology 2003;61:288–9.
[12] Emslie-Smith AM, Arahata K, Engel AG. Major histocompatibility class I antigen expression, immunolocalization of interferon subtypes, and T cell-mediated cytotoxicity in myopathies. Hum Pathol 1989;20:224–31.
[13] Pegoraro E, Mancias P, Swerdlow SH, et al. Congenital muscular dystrophy with primary laminin 2 (merosin) deficiency presenting as inflammatory myopathy. Ann Neurol 1996;40:782–91.
[14] Arahata K, Ishihara T, Fukunaga H, et al. Inflammatory response in facioscapulohumeral muscular dystrophy (FSHD): immunocytochemical and genetic analyses. Muscle Nerve 1995;2:S56–66.
[15] Gallardo E, Rojas-Garcia R, de Luna N, Pou A, Brown Jr RH, Illa I. Inflammation in dysferlin myopathy: immunohistochemical characterization of 13 patients. Neurology 2001;57:2136–8.
[16] Darin N, Kroksmark AK, Ahlander AC, et al. Inflammation and response to steroid treatment in limb-girdle muscular dystrophy 2I. Eur J Paediatr Neurol 2007;11:353–7.
[17] Thompson CE. Infantile Myositis. Dev Med Child Neurol 1982;24:307–13.
[18] Vajsar J, Jay V, Babyn P. Infantile myositis presenting in the neonatal period. Brain Dev 1996;18:415–9.
[19] McNeil SM, Woulfe J, Ross C, Tamopolsky MA. Congenital inflammatory myopathy: a demonstrative case and proposed diagnostic classification. Muscle Nerve 2002;25:259–64.
[20] Roddy SM, Ashwal S, Peckham N, Mortensen S. Infantile myositis: a case diagnosed in the neonatal period. Pediatr Neurol 1986;2:241–4.
[21] Mercuri E, Pichiecchio A, Allsop J, Messina S, Pane M, Muntoni F. Muscle MRI in inherited neuromuscular disorders: past, present, and future. J Magn Reson Imaging 2007;25:433–40.
[22] van Berlo JH, de Voogt WG, van der Kool AJ, et al. Meta-analysis of clinical characteristics of 299 carriers of *LMNA* gene mutations: do *lamin* A/C mutations portend a high risk of sudden death? J Mol Med 2005;83:79–83.
[23] Meune C, van Berlo JH, Anselme F, et al. Primary prevention of sudden death in patients with *lamin* A/C gene mutations. N Engl J Med 2006;354:209–10.

Human Molecular Genetics, 2011, Vol. 20, No. 19 **3841–3851**
doi:10.1093/hmg/ddr305
Advance Access published on July 12, 2011

Muscle choline kinase beta defect causes mitochondrial dysfunction and increased mitophagy

Satomi Mitsuhashi[1], Hideyuki Hatakeyama[2], Minako Karahashi[3], Tomoko Koumura[3], Ikuya Nonaka[1], Yukiko K. Hayashi[1], Satoru Noguchi[1], Roger B. Sher[4], Yasuhito Nakagawa[3], Giovanni Manfredi[5], Yu-ichi Goto[2], Gregory A. Cox[4] and Ichizo Nishino[1,*]

[1]Department of Neuromuscular Research and [2]Department of Mental Retardation and Birth Defect Research, National Institute of Neuroscience, National Center of Neurology and Psychiatry, Tokyo, Japan, [3]School of Pharmaceutical Sciences, Kitasato University, Tokyo, Japan, [4]The Jackson Laboratory, Bar Harbor, ME, USA and [5]Weil Medical College of Cornell University, New York, NY, USA

Received May 17, 2011; Revised and Accepted July 7, 2011

Choline kinase is the first step enzyme for phosphatidylcholine (PC) *de novo* biosynthesis. Loss of choline kinase activity in muscle causes rostrocaudal muscular dystrophy (*rmd*) in mouse and congenital muscular dystrophy in human, characterized by distinct mitochondrial morphological abnormalities. We performed biochemical and pathological analyses on skeletal muscle mitochondria from *rmd* mice. No mitochondria were found in the center of muscle fibers, while those located at the periphery of the fibers were significantly enlarged. Muscle mitochondria in *rmd* mice exhibited significantly decreased PC levels, impaired respiratory chain enzyme activities, decreased mitochondrial ATP synthesis, decreased coenzyme Q and increased superoxide production. Electron microscopy showed the selective autophagic elimination of mitochondria in *rmd* muscle. Molecular markers of mitophagy, including Parkin, PINK1, LC3, polyubiquitin and p62, were localized to mitochondria of *rmd* muscle. Quantitative analysis shows that the number of mitochondria in muscle fibers and mitochondrial DNA copy number were decreased. We demonstrated that the genetic defect in choline kinase in muscle results in mitochondrial dysfunction and subsequent mitochondrial loss through enhanced activation of mitophagy. These findings provide a first evidence for a pathomechanistic link between *de novo* PC biosynthesis and mitochondrial abnormality.

INTRODUCTION

Phosphatidylcholine (PC) is the major phospholipid in eukaryotic cell membranes. Disruption of PC synthesis by loss-of-function mutations in *CHKB* (GenBank Gene ID 1120), which encodes the primary choline kinase isoform in muscle, causes autosomal recessive congenital muscular dystrophy with mitochondrial structural abnormalities in human (1). Loss-of-function mutation in the murine ortholog, *Chkb*, is reported to cause rostrocaudal muscular dystrophy (*rmd*) in the laboratory mouse (2). *Rmd* is so-named because of a gradient of severity of muscle damage—hindlimbs (caudal) are affected more severely than forelimbs (rostral). The most outstanding feature of the muscle pathology in both human patients and *rmd* mice is a peculiar mitochondrial abnormality—mitochondria are greatly enlarged at the periphery of the fiber and absent from the center.

Mitochondria have a variety of cellular functions from energy production to triggering apoptotic cell death (3,4). Inhibition of mitochondrial respiration [chemically or by mitochondrial DNA (mDNA) mutations], disruption of inner membrane potential, senescence and enhanced reactive oxygen species (ROS) production are all known to cause mitochondrial morphological abnormalities (5–8). Conversely,

*To whom correspondence should be addressed at: Department of Neuromuscular Research, National Institute of Neuroscience, National Center of Neurology and Psychiatry, 4-1-1 Ogawahigashi-cho, Kodaira, Tokyo 187-8502, Japan. Tel: +81 423461712; Fax: +81 423461742; Email: nishino@ncnp.go.jp

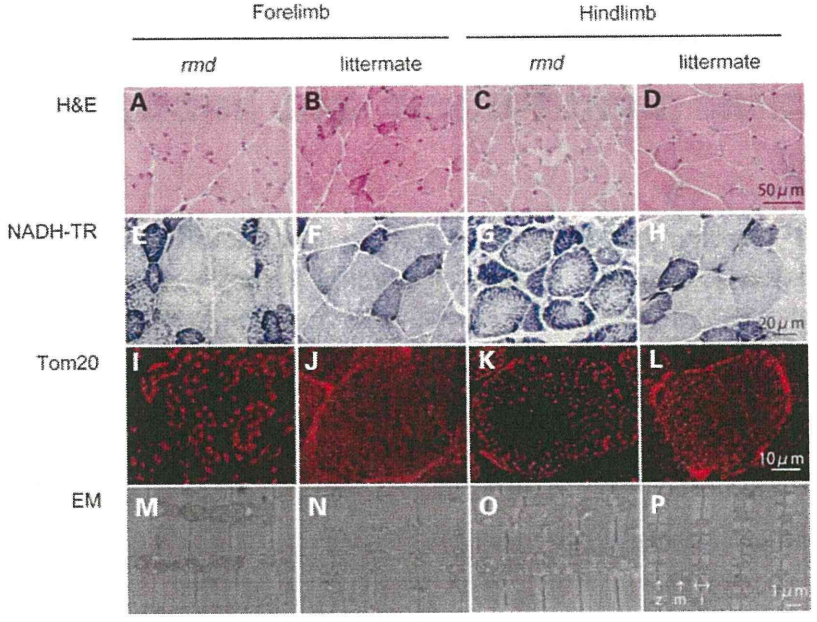

Figure 1. Muscle histopathology. H&E staining of triceps or quadriceps femoris muscles in 8-week-old homozygous *rmd* mutant mice and unaffected (+/*rmd* or +/+) littermate controls (**A**–**D**) shows dystrophic changes including variation in fiber size, necrosis and regeneration of individual fibers and interstitial fibrosis. NADH-TR staining (**E**–**H**), immunostaining of mitochondrial outer membrane protein Tom20 and EM (**M**–**P**) show abnormal mitochondria. Mitochondria in *rmd* muscle fibers are enlarged and prominent at the periphery, but sparse in the center (**I**–**L**). z, Z line; m, M line; i, I band.

primary mitochondrial morphological changes can subsequently cause mitochondrial and cellular dysfunction. Mitochondria are dynamic organelles, which continuously fuse and divide. Disequilibrium of mitochondrial fusion and fission can cause alterations of mitochondrial morphology with mitochondrial dysfunction (9,10). Thus, mitochondrial function and morphology are tightly linked.

It has been reported that mitochondria in *rmd* show decreased membrane potential (11). However, there have been no further studies about mitochondrial functional abnormalities in *rmd*, although its morphology is the most distinct feature compared with other myopathies. In addition, there has been no study about mitochondrial function when PC synthesis is blocked *in vivo*, although mitochondrial respiratory enzyme activities are dependent on membrane phospholipids (12). We hypothesized that the mitochondrial morphological abnormality in *rmd* muscle indicates the presence of a bioenergetic dysfunction caused by mitochondrial membrane phospholipid alteration.

In this study, we demonstrate that mitochondria in *rmd* mouse muscle show reduced PC level, bioenergetic dysfunction and increased ROS production are ubiquitinated and eliminated via mitophagy, leading to the peculiar mitochondrial loss in the skeletal muscle. These findings provide further evidence that mitochondrial dysfunction is related to phospholipid metabolism and may play a role in the pathogenesis of muscle disease.

RESULTS

Light microscopic examination of H&E-stained samples from 8-week-old homozygous *rmd* mutant mice and littermate controls confirmed dystrophic muscle pathology, especially in hindlimb muscles, as previously described (2) (Fig. 1A–D). NADH-TR and immunohistochemistry for mitochondrial outer membrane protein Tom20 also showed that mitochondria were sparse in the muscle fiber both in forelimb and hindlimb muscles of *rmd* mice, while the remaining mitochondria were prominent (Fig. 1E–L). More striking is the mitochondrial enlargement observed by EM (Fig. 1M–P). Mitochondria were rounder and massively enlarged compared with littermate controls. Normally, two mitochondria are present in almost all intermyofibrillar spaces and extend alongside the region between Z band and I bands. In muscles of *rmd* mice, mitochondria were larger than the size of the Z-I length itself, and often exceeded the size of a single sarcomere. In addition, mitochondria were seen only in some intermyofibrillar spaces leaving many regions devoid of mitochondria.

We hypothesized that the abnormal mitochondrial morphology in *rmd* skeletal muscles reflects altered PC content in mitochondrial membranes, as these mitochondria lack the PC biosynthetic pathway. We therefore measured PC, PE and CL in isolated mitochondria (Fig. 2). PE is the second most abundant phospholipid in mitochondria and CL is a mitochondria-specific phospholipid. PC was significantly decreased to 72% in forelimb and to 61% in hindlimb muscles compared with healthy littermates, while PE levels were unchanged. The PC/PE ratio was decreased, reflecting the PC reduction. This reduction is well correlated with the phospholipid compositional alteration in muscle tissue as previously described (1,2). CL showed only a slight decrease and only in the more severely affected hindlimb muscles.

We speculated that mitochondrial function in *rmd* is altered, and therefore measured respiratory enzyme activity and ATP

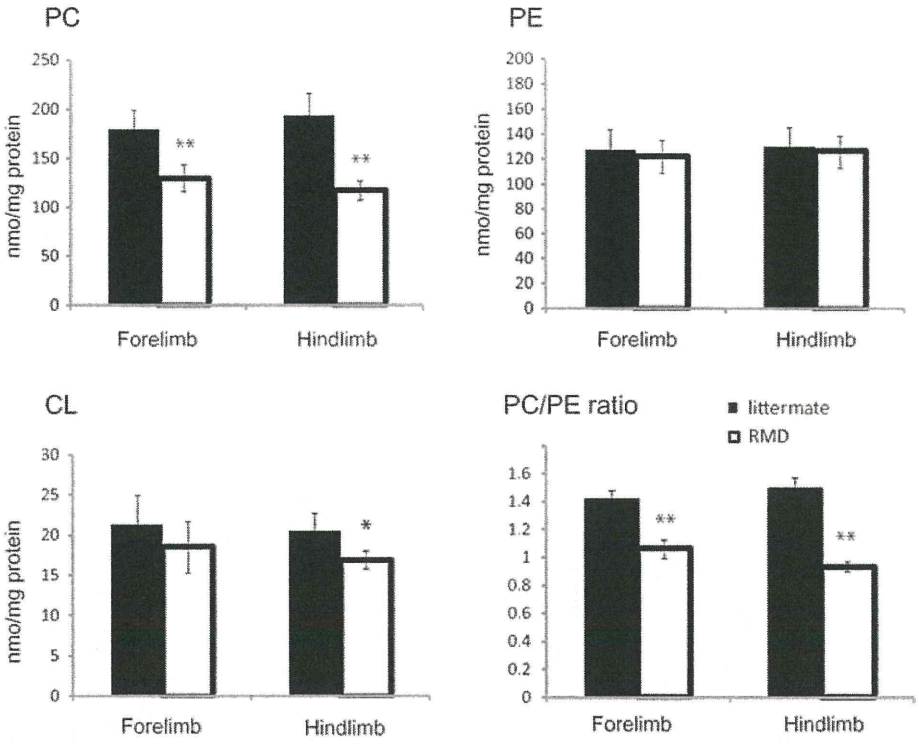

Figure 2. The PC level is decreased in *rmd* muscle mitochondria. The PE level is not altered. The PC/PE ratio is significantly decreased in *rmd*. The CL level is slightly decreased in *rmd* hindlimb. Data are expressed as the mean ± SD of eight experiments. $^{*}P < 0.01$, $^{**}P < 0.0001$.

synthesis in isolated mitochondria in *rmd* muscle. Compared with healthy littermates, only mitochondrial respiratory Complex III activity was significantly decreased in mitochondria from *rmd* forelimb muscles, while Complex I, III and IV activities were significantly decreased in *rmd* hindlimb muscles (Fig. 3A). Mitochondrial ATP synthesis was severely decreased, especially in hindlimb muscles (Fig. 3B), and coenzyme Q9 was moderately decreased in *rmd* compared with littermates (Fig. 3C).

In-gel activity staining on native PAGE showed decreased Complex III activity, especially in hindlimb (Fig. 4A), although normal protein levels of the Complex III were detected by western blot followed by Native PAGE (Fig. 4B). There was no difference in mobility of Complex III in *rmd* and littermate. Furthermore, respiratory chain supercomplex formation, which is important for effective electron transport (24), was not altered in *rmd* (Supplementary Material, Fig. S1).

Mitochondria are a major site of ROS production under normal circumstances and the production of ROS is enhanced when respiration is blocked. To determine whether the identified respiratory defects lead to elevated ROS, we measured superoxide levels from isolated mitochondria. Superoxide production was significantly increased in *rmd* muscle mitochondria, especially in those isolated from the hindlimbs (Fig. 5A). Moreover, the MDA level (Fig. 5B) and 4-hydroxynonenal adducts (Fig. 5C) were increased in *rmd* muscles indicating that oxidative stress is increased in *rmd* muscle.

Interestingly, examination of muscle sections by EM revealed autophagosomes selectively engulfing an entire mitochondrion, without cytoplasm, suggesting that mitophagy is activated in *rmd* skeletal muscles (Fig. 6A). Western blots of isolated mitochondria from muscle showed significantly increased levels of the autophagosome marker LC3 in *rmd* (Fig. 6B). In addition, polyubiquitinated proteins and p62/SQSTM1, which connects ubiquitination and autophagic machineries, were also increased in isolated mitochondria (Fig. 6B). These data suggest that mitochondria are polyubiquitinated and p62 is recruited to mitochondria. We also analyzed PINK1 and the E3 ubiquitin ligase Parkin, which are known to contribute to ubiquitination and mitophagy of damaged mitochondria (25,26). PINK1 and Parkin levels were increased in *rmd* isolated muscle mitochondria (Fig. 6B), suggesting that they were recruited to mitochondria to promote mitophagy. Immunohistochemical analyses demonstrated the colocalization of p62, polyubiquitin and LC3 with mitochondria (Fig. 6C).

We quantified mitochondrial numbers in muscle fibers, mitochondria occupying-area relative to muscle cross-sectional area and mean mitochondrial area in cross-section by morphometric analysis in EM. In *rmd*, the average number of mitochondria per fiber was profoundly decreased (Fig. 7A). However, the average area occupied by mitochondria in each muscle fiber was comparable with littermates (Fig. 7A). This was due to increased mean mitochondrial area in *rmd* (Fig. 7A).

We quantified mtDNA copy number relative to nuclear DNA. In *rmd*, mtDNA was decreased both in forelimb and

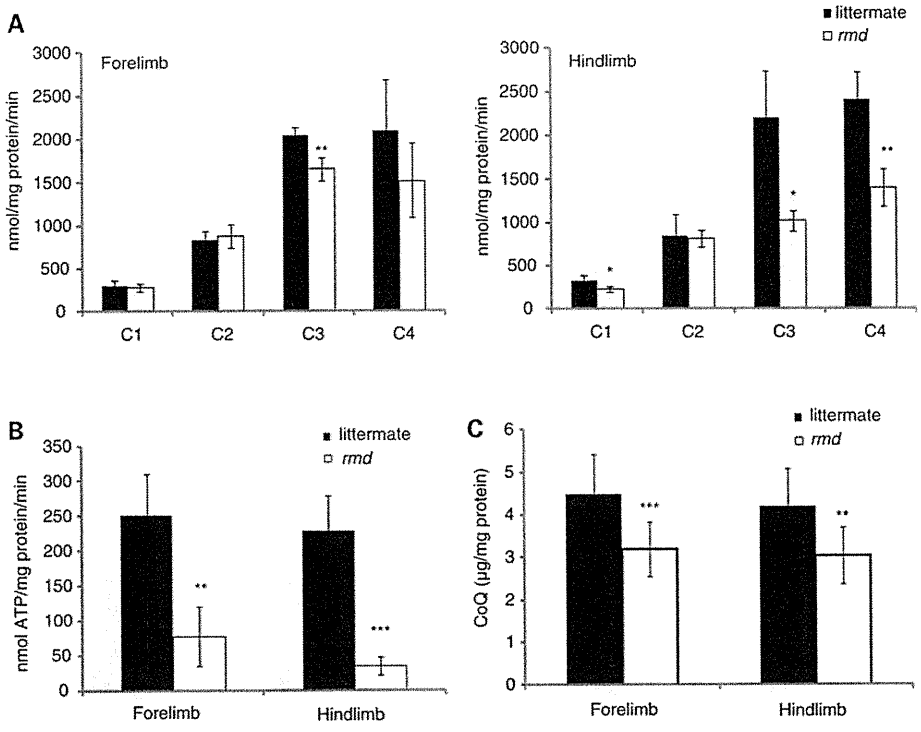

Figure 3. Mitochondrial energetic function is altered and CoQ level is decreased in *rmd*. (**A**) Mitochondrial respiratory chain enzyme activities in *rmd* were compared with healthy littermates. C1, Complex I ; C2, Complex II ; C3, Complex III ; C4, Complex IV ($n = 4$). (**B**) The rate of ATP synthesis measured by luminometry method ($n = 4$). (**C**) Total CoQ9 level (littermate forelimb, $n = 13$; littermate hindlimb, $n = 12$; *rmd* forelimb, $n = 11$; *rmd* hindlimb, $n = 13$). Data are expressed as the mean ± SD of experiment number shown as *n*. $^{*}P < 0.05$, $^{**}P < 0.005$, $^{***}P < 0.001$.

hindlimb muscles compared with littermate controls (Fig. 7B), which was in agreement with the number of mitochondria decrease. The mtDNA copy number in liver is preserved in *rmd*, and reduction in muscle is progressive in age.

DISCUSSION

In the *rmd* mouse, we observed greater superoxide production and more significant Complex III and ATP synthesis deficiencies in hindlimb than in forelimb muscles, correlating with the more severe caudal phenotype. PC was decreased in isolated *rmd* muscle mitochondria as a consequence of disruption of muscle PC biosynthesis because PC cannot be synthesized in mitochondria. This suggests that muscle damage in the *rmd* mouse is primarily due to mitochondrial dysfunction possibly caused by the impaired PC biosynthesis.

Why then are mitochondrial functions altered when PC is decreased? Mitochondria produce energy mainly via oxidative phosphorylation, which transfers electrons by a series of redox reactions through four enzyme complexes, and pumps protons across the mitochondrial inner membrane, producing an electrochemical proton gradient that enables ATP synthesis (3). Here, we demonstrate for the first time a Complex III activity decrease without the loss of the enzyme protein complex in *rmd* muscle mitochondria, suggesting a link between decreased PC content and Complex III activity. One possible explanation is that mitochondrial PC alterations may directly impair Complex III function by affecting lipid–protein interactions (27). PC is a component of the yeast respiratory enzyme complex, as revealed by X-ray crystallography, and thus may regulate enzyme function (28). Alteration of fatty acid composition in PC has been shown to change enzymatic activity in Complexes I, III and IV in a mouse model (29). In this model, Complex III activity is profoundly increased when n-3 fatty acid is increased. In *rmd*, it is reported that docosahexiaenoic acid containing PC, the major n-3 fatty acid in muscle PC, is profoundly decreased in muscle and in isolated mitochondria (1). This suggests a possible association between phospholipid composition alterations and respiratory chain enzymatic activities due to the choline kinase defect in *rmd* muscle.

Through the oxidative phosphorylation process, ROS are also generated as byproducts even in normal cellular states, but especially when respiration is inhibited (30,31). In *rmd* mouse muscle, ROS production from isolated mitochondria was increased, which may be related to the respiratory chain defect caused by PC reduction in mitochondria. Interestingly, selenium-deficient myopathy is associated with muscle pathology showing similar enlarged and sparse mitochondrial morphological abnormalities to the *rmd* mice and the human congenital muscular dystrophy caused by *CHKB* mutations (32). As selenium is a cofactor of glutathione peroxidase, selenium deficiency is thought to cause oxidative stress (33,34). Morphological similarity between choline kinase beta deficiency and selenium deficiency suggests that ROS may play a key role in the formation of the mitochondrial

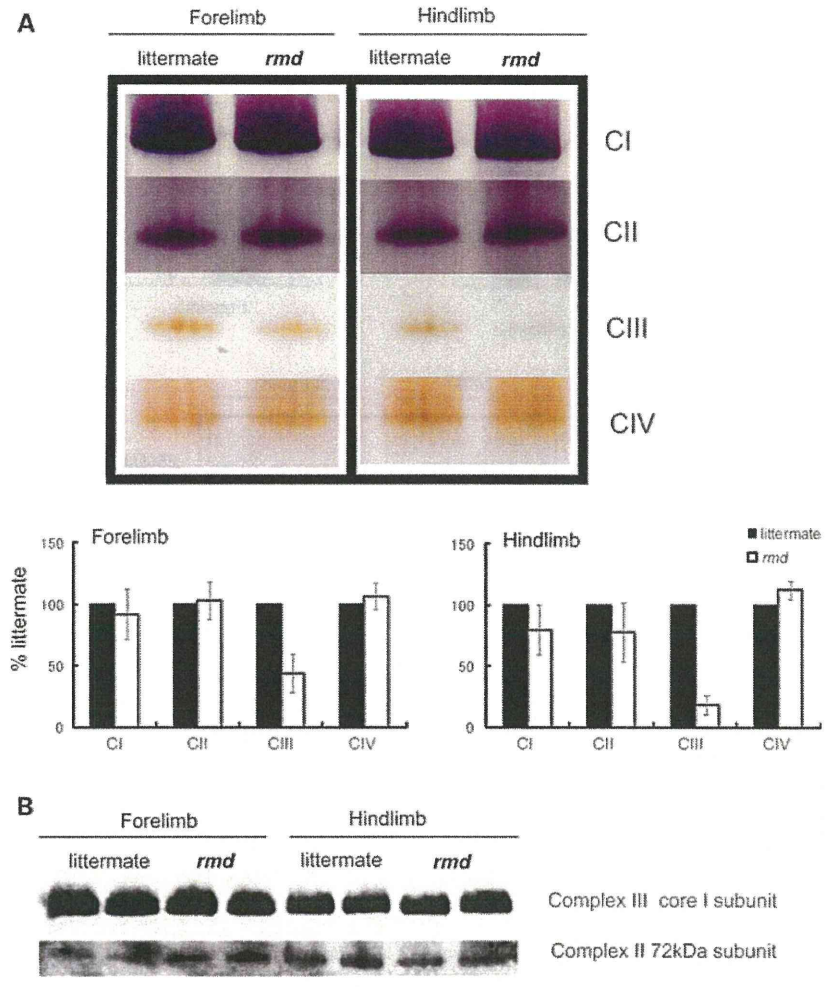

Figure 4. Mitochondrial respiratory enzyme activity is decreased without the loss of the enzyme complex. (**A**) Native PAGE gel electrophoresis. In-gel activity staining shows that Complex III activity is decreased in *rmd*. Representative data from four different experiments are shown. (**B**) Immunoblotting of Complex II and III shows protein levels are maintained despite defect in significant Complex III enzymatic activity. Representative data from three different experiments of six samples are shown.

abnormalities in *rmd* myopathy. In another model, depletion of glutathione, which provides cells with a reducing environment and detoxifies the ROS, is reported to cause mitochondria enlargement in muscle, also suggesting the possible link between mitochondrial enlargement and ROS in skeletal muscle (35).

In addition, as a major site of ROS production, mitochondria themselves are prone to ROS damage (36). Recent studies have shown that damaged mitochondria are eliminated by selective autophagy, called mitophagy, most likely as a quality control mechanism to protect the cells (37,38). In addition to mitochondrial enlargement, we observed large areas devoid of mitochondria. Mitochondrial depolarization can trigger mitophagy in cell culture models (26). PINK1 and Parkin interactions promote ubiquitination of mitochondrial outer membrane proteins, and induce mitophagy. This process is mediated by p62, an adaptor molecule, which interacts directly with ubiquitin and LC3 (25,39). ROS generated from mitochondria are also important for mitophagy (39). Interestingly, we found increased mitophagy in *rmd*, accompanied by mitochondrial ubiquitination and recruitment of p62 and LC3. Enhanced PINK1 and Parkin expression in mitochondria likely reflects the process of elimination of damaged mitochondria as a consequence of mitochondrial dysfunction and ROS production. These findings were similar to those in cells treated with the protonophore carbonyl cyanide m-chlorophenyl hydrazone (CCCP) or respiratory chain inhibitors (25,26). In *rmd*, decreased membrane potential (11), as a consequence of respiratory chain insufficiency and ROS production, may trigger mitophagy and thus increased mitochondrial clearance, which may lead to energy crisis and result in cell death and muscular dystrophy.

We observed progressive loss of mtDNA with age, together with progressive loss of mitochondria. We suggest that mtDNA depletion in this case results from increased mitophagy, because mtDNA is known to be degraded by mitophagy in cultured hepatocytes (40) and because the pathological features of CHKB-deficient myopathy are clearly distinct from those

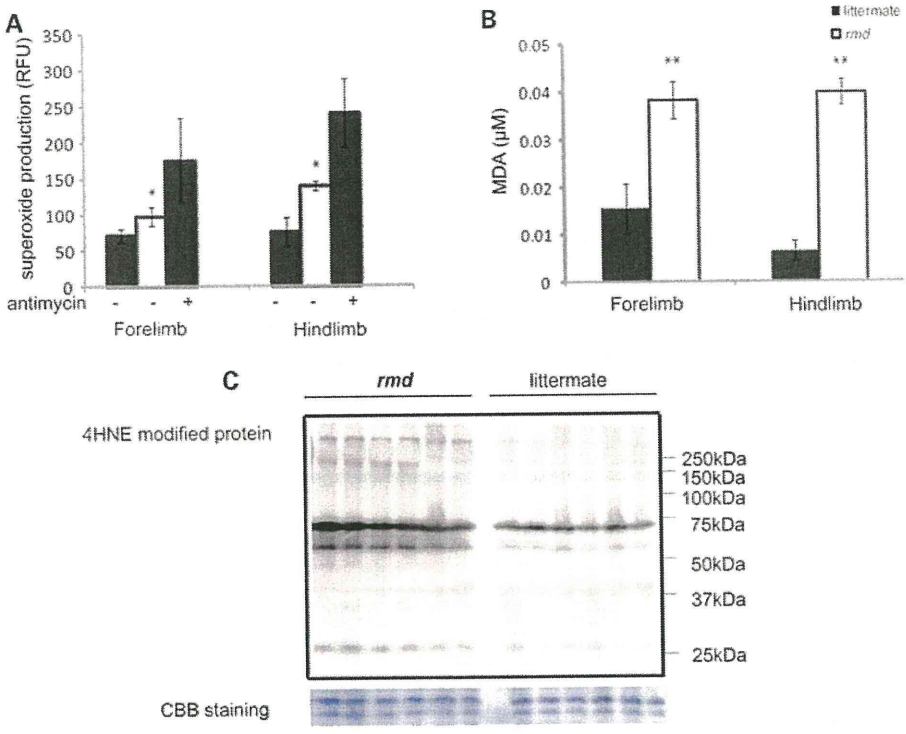

Figure 5. Mitochondrial superoxide production is increased and oxidative stress is increased in muscle tissue in *rmd*. (**A**) Mitochondrial superoxide production is enhanced in *rmd*, especially in hindlimb muscle mitochondria. Data are shown as the mean ± SD of seven experiments. $^{*}P < 0.001$. (**B**) MDA levels are increased in muscle tissue. $^{**}P < 0.0005$. Data are shown as the mean ± SD ($n = 4$ for *rmd* and $n = 5$ for littermate controls). (**C**) HNE4-modified proteins are increased in *rmd* hindlimb muscle. Coomassie brilliant blue staining is shown as a loading control. Representative data of six samples.

observed in 'primary' mtDNA depletion syndromes, usually associated with defective mtDNA synthesis, in which muscle fiber mitochondria are increased both in number and size, causing the 'ragged-red fiber' appearance (41).

In summary, we have demonstrated for the first time a pathogenic mechanism that links PC reduction in the mitochondrial membranes of *rmd* muscle to mitochondrial morphological and functional abnormalities and the induction of mitophagy as a response to structural and functional damage by ROS generation or impaired bioenergetics. These findings indicate the importance of PC *de novo* synthesis pathway and phospholipid composition of mitochondrial membrane in the maintenance of mitochondria and muscle.

MATERIALS AND METHODS

Rmd mice

Eight-week-old *rmd* mice (2) were used for all analysis and were compared with healthy littermates. The Ethical Review Committee on the Care and Use of Rodents in the National Institute of Neuroscience, National Center of Neurology and Psychiatry approved all mouse experiments.

Histological analyses

The quadriceps femoris muscles were freeze-fixed in liquid-nitrogen-cooled isopentane and stored at −80°C. Serial transverse sections of 10 μm thickness were stained with a series of histochemical methods, including hematoxylin and eosin (H&E) and nicotine amide adenine dinucleotide-tetrazolium reductase (NADH-TR), as previously described (13), and were observed by light microscopy.

Immunohistochemical analyses were performed as previously described (13). Briefly, 6 μm thick frozen muscle sections were fixed in cold acetone for 5 min. After blocking with 5% normal goat serum, sections were incubated with primary antibodies for 2 h at 37°C. After rinses with phosphate-buffered saline, sections were incubated with secondary Alexa Fluor 488- or Alexa Fluor 568-labeled goat anti-mouse

Figure 6. Mitochondrial degeneration in *rmd*. (**A**) EM of extensor digitorum longus muscle. In *rmd*, mitochondria are degraded by mitophagy. Scale bar = 0.5 μm. (**B**) Western blot of isolated muscle mitochondria immunodetected for Parkin, polyubiquitin, p62/SQSTM1 and LC3. TOM20, a mitochondrial outer membrane protein is used as loading control. Hindlimb mitochondria in *rmd* show significantly increased expression level in these mitophagy markers. (**C**) p62 and TOM20 immunohistochemistry of hindlimb muscle section. Note that mitochondria are significantly enlarged and sparse in *rmd*. p62 colocalizes with the mitochondrial outer membrane protein TOM20. Polyubiquitin and mitochondrial protein cytochrome c oxidase (COX) colocalize. LC3 and TOM20 colocalize. Polyubiquitin and p62 colocalize. Scale bar = 10 μm.

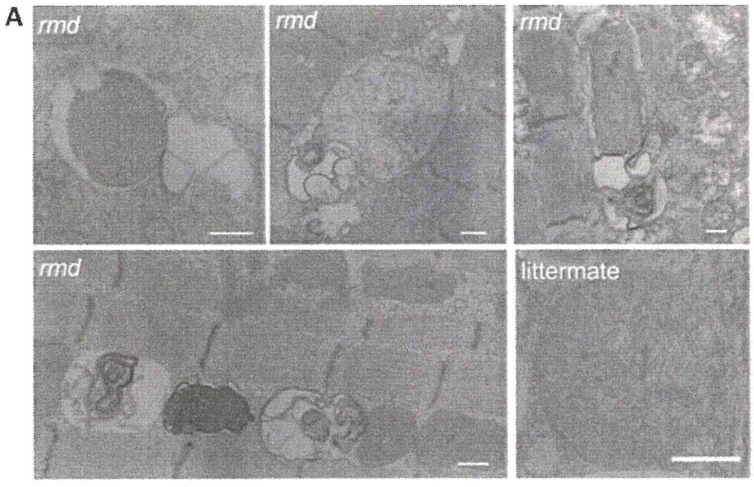

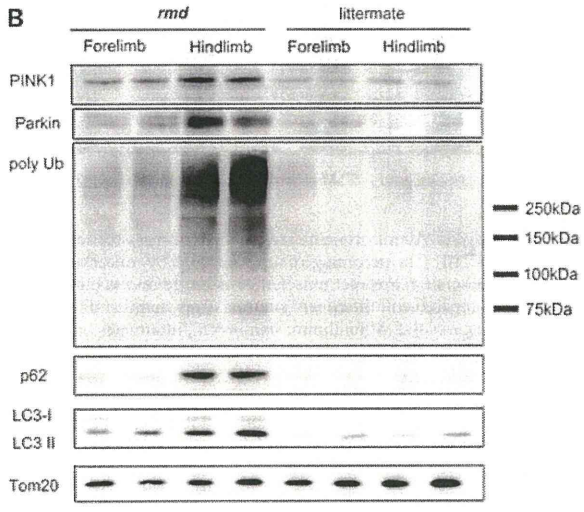

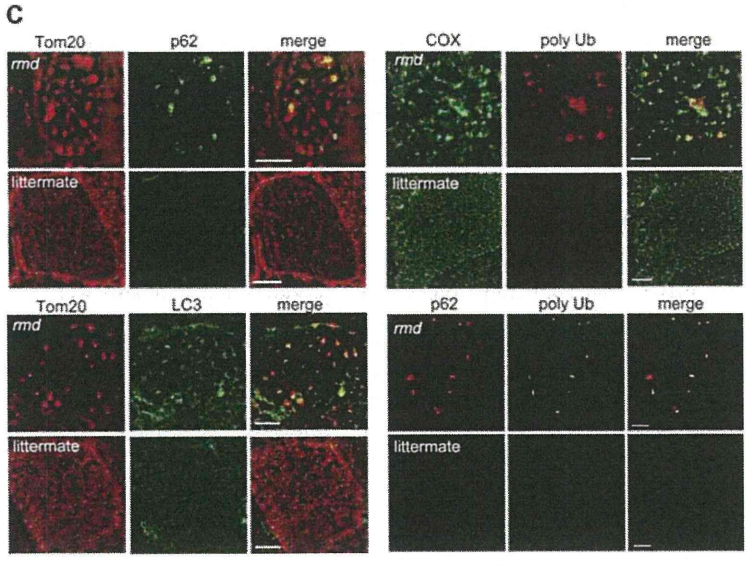

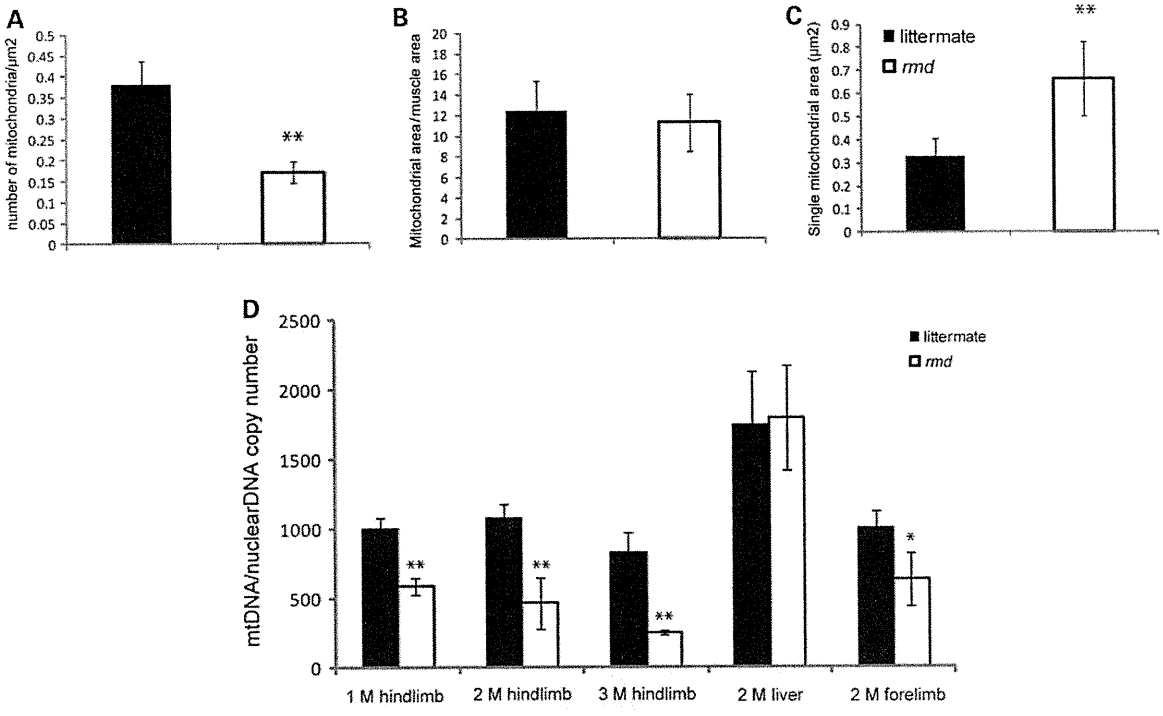

Figure 7. (**A**) Mitochondrial morphometrical analysis. All mitochondria are counted in cross-sections of EDL muscle by EM. Number of mitochondria per 1 μm^2 of muscle fiber cross-sectional area is shown ($n = 20$). The percentage of area occupied by mitochondria in a cross-section of muscle fiber is not different in *rmd* and littermates ($n = 20$). The average total mitochondrial area per muscle fiber is larger in *rmd* compared with littermates ($n = 20$). $^{*}P < 0.005$, $^{**}P < 0.0005$. (**B**) mtDNA copy number is decreased in *rmd* compared with littermate controls. Copy number of mtDNA (ND1) was normalized by nuclear DNA (*pcam1*) (M; month-old, 1 M hindlimb: *rmd*; $n = 4$, littermates; $n = 4$. 2 M hindlimb: *rmd*; $n = 5$, littermates; $n = 6$, 3 M hindlimb: *rmd*; $n = 4$, littermates; $n = 6$. 2 M liver: *rmd*; $n = 5$, littermates; $n = 5$. 2 M forelimb: *rmd*; $n = 6$, littermates; $n = 6$).

or rabbit antibodies at room temperature for 45 min. Confocal images were obtained with FLUOVIEW FV500 systems (Olympus) using a ×100 objective.

For observation by electron microscopy (EM), muscle samples were fixed in 2.5% glutaraldehyde in 0.1 M cacodylate buffer. Specimens were post-fixed in 1% osmium tetroxide in the same buffer, dehydrated with graded series of ethanol and embedded in epon, as previously described (13). Ultrathin sections were stained with uranyl acetate and lead citrated, and were analyzed by a FEI Tecnai Spirit at 120 kV.

Isolation of skeletal muscle mitochondria

Mitochondria from skeletal muscle of whole forelimb and hindlimbs were isolated by differential centrifugation. Fresh muscle was minced and homogenized using a motor-driven Teflon pestle homogenizer with ice-cold mitochondrial isolation buffer [10 mM Tris–HCl pH 7.2, 320 mM sucrose, 1 mM ethylenediaminetetraacetic acid, 1 mM dithiothreitol, 1 mg/ml bovine serum albumin (BSA)] and centrifuged at 1500*g* for 5 min. Supernatant fraction was centrifuged at 15 000*g* for 20 min, and the pellet was resuspended in mitochondrial isolation buffer. The centrifugation was repeated twice. Protein concentration was determined by the Bradford method using Bio-Rad Protein Assay (Bio-Rad Laboratories), according to the manufacturer's protocol.

Lipid extraction, phospholipid separation and determination

PC, phosphatidylethanolamine (PE) and cardiolipin (CL) were extracted from isolated mitochondria of forelimb and hindlimb muscles, separated by one-dimensional thin layer chromatography (TLC) and amount of each phospholipid was measured by phosphorus analysis (14,15). Briefly, total lipids in frozen muscle biopsy samples were extracted according to the method of Bligh and Dyer (14). Each extract was evaporated to dryness under nitrogen, and the residues were then dissolved in a small amount of a 2:1 v/v mixture of chloroform and methanol and applied to a TLC plate (Merck, Silica Gel 60). The plate was developed with a medium of chloroform:-methanol:formic acid:acetic acid = 100:100:9:9 (v/v/v/v). The products and standards were visualized with primulin reagent, and the products identified by comparison with chromatographic standards. PC and PE were then scraped from the TLC plate for quantification. Phospholipids were quantified according to the method of Rouser *et al.* (15). Briefly, the lipids were digested by heating for 1 h at 200°C with 70% perchloric acid. After cooling, ammonium molybdate and ascorbic acid solution were added in that order. Color was developed after heating for 5 min in a boiling water bath. Absorbance was determined at 820 nm by spectrophotometer. Phospholipid levels were corrected by the total protein amount in isolated mitochondria.

Respiratory enzyme activity and ATP synthesis

Mitochondrial respiratory enzyme activities were measured as previously described, using colorimetric assays in isolated mitochondria (16,17). Complex I (NADH-ubiquinone oxidoreductase) activity was measured by the reduction of 10 μM decylubiquinone (DB) in the presence of 2 mM potassium cyanide (KCN), 50 μg/ml antimycin and 50 μM NADH at 272 nm. Complex II (succinate-ubiquinone oxidoreductase) activity was measured by the reduction of 50 μM 2,6-dichlorophenolindophenol in the presence of 20 mM succinate, 2.5 μg/ml rotenone, 2.5 μg/ml antimycin, 2 mM KCN and 50 μM DB at 600 nm. Complex III (ubiquinol-ferricytochrome c oxidoreductase) activity was measured by the reduction of 50 μM cytochrome c at 550 nm in the presence of 50 μM reduced DB and 2 mM KCN. Complex IV (ferrocytochrome c-oxigen oxidoreductase) activity was measured by the oxidation of 2.5 μM reduced cytochrome c at 550 nm. The activity was calculated using an extinction coefficient of 8 $mM^{-1} cm^{-1}$, 19.1 $mM^{-1} cm^{-1}$, 19.0 $mM^{-1} cm^{-1}$ and 19.0 $mM^{-1} cm^{-1}$ for Complexes I, II, III and IV, respectively. The specific activity of the enzymes was expressed as nmol of each substrate oxidized or reduced/min/mg of mitochondrial protein.

Mitochondrial ATP synthesis was measured by the method of Manfredi and colleagues (18). Briefly, isolated mitochondria were resuspended in 0.25 M sucrose, 50 mM 4-(2-hydroxyethyl)-1-piperazineethanesulfonic acid (HEPES), 2 mM $MgCl_2$, 1 mM ethylene glycol tetraacetic acid (EGTA) and 10 mM KH_2PO_4, pH 7.4. Then 0.15 mM P1,P5-di(adenosine) pentaphosphate, 1 mM malate, 1 mM pyruvate, luciferin and luciferase and 0.1 mM adenosine diphosphate (ADP) were added, and light emission was recorded by luminometer. For each sample, 1 mM oligomycin-added sample was used to obtain the baseline luminescence corresponding to non-mitochondrial ATP production.

CoQ9 determination

Total CoQ9 contents in isolated mitochondria were analyzed with high performance liquid chromatography (HPLC) by electrochemical detection according to the standard procedure described by Tang *et al.* (19). Briefly, isolated muscle mitochondria pellet were lysed with 2-propanol, vortexed for 1 min and centrifuged at 2000*g* for 10 min and then clear supernatant was applied for HPLC Coul Array Detector Model 5600A (ESA BIOSCIENCES, Inc.) with Capcell Pak C18 MG 100 column (3.2 I.D × 150 mm length; ESA BIOSCIENCES, Inc.). The mobile phase was degassed methanol containing 0.4% sodium acetate, 1.5% acetic acid, 1% 2-propanol and 8% n-hexane. Chromatographic data were analyzed with CoulArray Data Station 3.00 (ESA Biosciences). Standard curves were created with both oxidized and reduced CoQ9. Total CoQ9 level was determined according to the standard curve and corrected by the total protein level in isolated mitochondria as measured by the Bradford method.

High-resolution clear native PAGE

High-resolution clear native polyacrylamide gel electrophoresis (PAGE) was performed by the method of Wittig *et al.* (20). Briefly, isolated mitochondria were solubilized with Native PAGE Sample buffer (Invitrogen) containing 0.3% n-dodecyl-β-D-maltoside (Dojindo). Twenty micrograms of protein were applied to 3–12% NativePAGE Bis–Tris gel (Invitrogen). Native PAGE buffer (Invitrogen) was used for anode buffer and Native PAGE buffer containing 0.02% n-dodecyl-β-D-maltoside and 0.05% deoxycolate was used for cathode buffer.

For in-gel catalytic activity assays, gels were incubated in the following solutions: Complex I, 5 mM Tris–HCl pH 7.4, 140 μM NADH and 3 mM nitro tetrazolium blue (NTB); Complex II, 5 mM Tris–HCl pH 7.4, 20 mM succinate, 3 mM NTB and 200 μM phenazine methosulfate; Complex III, 50 mM sodium phosphate buffer pH 7.2 and 0.5 mg/ml diaminobenzidine (DAB); Complex IV, 50 mM sodium phosphate buffer (pH 7.2), 0.5 mg/ml DAB and 5 mM cytochrome c.

For immunoblotting, gels were incubated for 20 min in 300 mM Tris, 100 mM acetic acid, 1% sodium dodecyl sulfate (SDS), pH 8.6 and then electroblotted to polyvinylidene fluoride (PVDF) membrane (Millipore). Complexes II and III were detected with monoclonal antibodies against the 70 kDa subunit (Abcam) and core 2 subunit (Invitrogen), respectively.

Measurement of mitochondrial superoxide (O_2^-) production

Mitochondrial superoxide production was measured by dehydroethidium (DHE) (Molecular Probes), as described previously (21). Isolated mitochondria were incubated with 200 mM mannitol, 70 mM sucrose, 2 mM HEPES pH 7.4, 0.5 mM EGTA and 0.1% BSA. Reagents were added in the following order: 1 mM glutamate, 1 mM malate, 1 μM DHE, 0.25 mM ADP and 5 mM KH_2PO_4. Fluoresence was measured by Cytofluor 4000 (Applied biosystems) at excitation/emission = 530/620 nm.

Measurement of malondialdehyde in muscle

Malondialdehyde (MDA) levels were measured in muscle homogenates using an LPO-485 assay kit (BIOXYTEC), according to the manufacturer's protocol.

Western blot analysis for muscle tissue and isolated mitochondria

Proteins were extracted from quadriceps femoris muscles or mitochondria isolated from forelimb and hindlimb muscles and suspended in SDS sample buffer; 125 mM Tris–HCl pH 6.8, 5% β-mercaptoethanol, 2% SDS and 10% glycerol. Extracted proteins were separated on acrylamide gels, and then transferred onto PVDF membranes (Millipore). Blocking solution of 5% skim milk was used. ImageQuant LAS 4000 Mini Biomolecular Imager (GE Healthcare) was used for evaluating bands.

Quantification of mtDNA by real-time PCR

Total DNA was isolated from triceps and quadriceps femoris and liver by proteinase K digestion and standard phenol–chloroform

extraction. Copy number of mtDNA (ND1) was quantified by real-time polymerase chain reaction (PCR) using SYBR Green PCR Kit (Qiagen) with *pcam1* as the control for the nuclear genome copy number. We used the following primers: ND1 forward primer, CCTATCACCCTTGCCATCAT; ND1 reverse primer, GAGGCTGTTGCTTGTGTGAC; *pcam1* DNA forward primer, ATGGAAAGCCTGCCATCATG; *pcam1* DNA reverse primer, TCCTTGTTGTTCAGCATCAC.

The amount of mtDNA relative to nuclear DNA was calculated using the following formula: mtDNA/nuclear DNA $= 2^{-(Ct_{mtDNA} - Ct_{nuclerDNA})}$ where Ct is the threshold cycle (22).

Morphometrical analysis of mitochondria

Cross-sectional EM image of extensor digitorum longus (EDL) muscle from *rmd* and littermates was analyzed by Image J software (23). Total areas of all mitochondria in 20 muscle fibers were calculated and compared with cross-sectional fiber areas. Total number of mitochondria per muscle fiber was counted.

Antibodies

Primary antibodies used were: mouse anti-4-hydroxy-2-nonenal (4-HNE) modified protein antibody (HNEJ-2,JalCA), rabbit anti-PINK1 antibody (BC100-494, Novus Biologicals), mouse anti-Parkin antibody (4211, Cell Signaling), rabbit anti-p62/SQSTM1 antibody (PWS860, Biomol), rabbit anti-LC3 antibody (NB100-2220, Novus Biologicals), mouse anti-poly-ubiquitin antibody (FK1, Biomol), rabbit anti-TOM20 antibody (FL-145, Santa Cruz), mouse anti-COX subunit 1 antibody (Invitrogen) and mouse anti-VDAC antibody (20B12, Santa Cruz). Second antibodies used were: horse radish peroxidase-labeled goat anti-mouse (Beckman Coulter) or rabbit antibodies (Cell Signaling), Alexa Fluor 488- and Alexa Fluor 568-labeled goat anti-mouse or rabbit antibodies (Invitrogen).

Statistical analysis

Data are presented as mean ± SD. Mean differences were compared with the analysis of *t*-test using R software version 2.11.0 (http://www.r-project.org/).

SUPPLEMENTARY MATERIAL

Supplementary Material is available at *HMG* online.

ACKNOWLEDGEMENTS

We thank Megumu Ogawa, Kanako Goto and Junko Takei for technical assistance.

FUNDING

This study was supported partly by the Research on Psychiatric and Neurological Diseases and Mental Health of Health and Labour Sciences Research Grants; partly by the Research on Intractable Diseases of Health and Labor Sciences Research Grants; partly by the Research Grant for Nervous and Mental Disorders (20B-12, 20B-13) from the Ministry of Health, Labour and Welfare; partly by an Intramural Research Grant (23-4, 23-5) for Neurological and Psychiatric Disorders from NCNP; partly by KAKENHI (20390250, 22791019); partly by Research on Publicly Essential Drugs and Medical Devices of Health and Labor Sciences Research Grants; partly by the Program for Promotion of Fundamental Studies in Health Sciences of the National Institute of Biomedical Innovation (NIBIO); and partly by the Grant from Japan Foundation for Neuroscience and Mental Health. G.A.C. and R.B.S. were supported in part by a National Institutes of Health Grant (AR054170 to G.A.C.).

REFERENCES

1. Mitsuhashi, S., Ohkuma, A., Talim, B., Karahashi, M., Koumura, T., Aoyama, C., Kurihara, M., Quinlivan, R., Sewry, C., Mitsuhashi, H. *et al.* (2011) A congenital muscular dystrophy with mitochondrial structural abnormalities caused by defective de novo phosphatidylcholine biosynthesis. *Am. J. Hum. Genet.*, **88**, 845–851.
2. Sher, R.B., Aoyama, C., Huebsch, K.A., Ji, S., Kerner, J., Yang, Y., Frankel, W.A., Hoppel, C.A., Wood, P.A., Vance, D.E. *et al.* (2006) A rostrocaudal muscular dystrophy caused by a defect in choline kinase beta, the first enzyme in phosphatidylcholine biosynthesis. *J. Biol. Chem.*, **281**, 4938–4948.
3. Saraste, M. (1999) Oxidative phosphorylation at the fin de siècle. *Science*, **283**, 1488–1493.
4. Spierings, D., McStay, G., Saleh, M., Bender, C., Chipuk, J., Maurer, U. and Green, D.R. (2005) Connected to death: the (unexpurgated) mitochondrial pathway of apoptosis. *Science*, **310**, 66–67.
5. Wakabayashi, T. (2002) Megamitochondria formation—physiology and pathology. *J. Cell Mol. Med.*, **6**, 497–538.
6. Benard, G., Bellance, N., James, D., Parrone, P., Fernandez, H. and Letellier, T. (2007) Mitochondrial bioenergetics and structural network organization. *J. Cell Sci.*, **120**, 838–848.
7. Yoon, Y.S., Yoon, D.S., Lim, I.K., Yoon, S.H., Chung, H.Y., Rojo, M., Malka, F., Jou, M.J., Martinou, J.C. and Yoon, G. (2006) Formation of elongated giant mitochondria in DFO-induced cellular senescence: involvement of enhanced fusion process through modulation of Fis1. *J. Cell Physiol.*, **209**, 468–480.
8. Karbowski, M., Kurono, C., Wozniak, M., Ostrowski, M., Teranishi, M., Nishizawa, Y., Usukura, J., Soji, T. and Wakabayashi, T. (1999) Free radical-induced megamitochondria formation and apoptosis. Free Radic. Biol. Med., **26**, 396–409.
9. Chen, H., Detmer, S.A., Ewald, A.J., Griffin, E.E., Fraser, S.E. and Chan, D.C. (2003) Mitofusins Mfn1 and Mfn2 coordinately regulate mitochondrial fusion and are essential for embryonic development. *J. Cell Biol.*, **160**, 189–200.
10. Chen, H., Chomyn, A. and Chan, D.C. (2005) Disruption of fusion results in mitochondrial heterogeneity and dysfunction. *J. Biol. Chem.*, **280**, 26185–26192.
11. Wu, G., Sher, R.B., Cox, G.A. and Vance, D.E. (2009) Understanding the muscular dystrophy caused by deletion of choline kinase beta in mice. *Biochim. Biophys. Acta*, **1791**, 347–356.
12. Daum, G. (1985) Lipids of mitochondria. *Biochim. Biophys. Acta*, **822**, 1–42.
13. Hayashi, Y.K., Matsuda, C., Ogawa, M., Goto, K., Tominaga, K., Mitsuhashi, S., Park, Y.E., Nonaka, I., Hino-Fukuyo, N., Haginoya, K. *et al.* (2009) Human PTRF mutations cause secondary deficiency of caveolins resulting in muscular dystrophy with generalized lipodystrophy. *J. Clin. Invest.*, **119**, 2623–2633.
14. Bligh, E.G. and Dyer, W.J. (1959) A rapid method of total lipid extraction and purification. *Can. J. Biochem. Physiol.*, **37**, 911–917.
15. Rouser, G., Fkeischer, S. and Yamamoto, A. (1970) Two dimensional then layer chromatographic separation of polar lipids and determination of phospholipids by phosphorus analysis of spots. *Lipids*, **5**, 494–496.
16. Mimaki, M., Hatakeyama, H., Ichiyama, T., Isumi, H., Furukawa, S., Akasaka, M., Kamei, A., Komaki, H., Nishino, I., Nonaka, I. *et al.* (2009)

Different effects of novel mtDNA G3242A and G3244A base changes adjacent to a common A3243G mutation in patients with mitochondrial disorders. *Mitochondrion*, **9**, 115–122.
17. Trounce, I.A., Kim, Y.L., Jun, A.S. and Wallace, D.C. (1996) Assessment of mitochondrial oxidative phosphorylation in patient muscle biopsies, lymphoblasts, and tranmitochondrial cell lines. *Methods enzymol.*, **264**, 484–509.
18. Vives-Bauza, C., Yang, L. and Manfredi, G. *Methods in Cell Biology. Mitochondria*, 2nd edn. Academic Press, London, UK, Vol. 80, Part 2, 7, 155–171.
19. Tang, P.H., Miles, M.V., Miles, L., Quinlan, J., Wong, B., Wenisch, A. and Bove, K. (2004) Measurement of reduced and oxidized coenzyme Q9 and coenzyme Q10 levels in mouse tissues by HPLC with coulometric detection. *Clin. Chim. Acta*, **341**, 173–184.
20. Wittig, I., Karas, M. and Schagger, H. (2007) High resolution clear native electrophoresis for in-gel functional assays and fluorescence studies of membrane protein complexes. *Mol. Cell Proteomics*, **6**, 1215–1225.
21. Armstrong, J.S. and Whiteman, M. *Methods in Cell Biology. Mitochondria*, 2nd edn. Academic Press, London, UK, Vol. 80, 18, 355–377.
22. Naini, A. and Shanske, S. *Methods in Cell Biology. Mitochondria*, 2nd edn. Academic Press, London, UK, Vol. 80, Part2, 22, 448–449.
23. Abramoff, M.D., Magelhaes, P.J. and Ram, S.J. (2004) Image processing with Image J. *Biophotonics Int.*, **11**, 36–42.
24. Zhang, M., Mileykovskaya, E. and Dowhan, W. (2002) Gluing the respiratory chain together. Cardiolipin is required for supercomplex formation in the inner mitochondrial membrane. *J. Biol. Chem.*, **277**, 43553–43556.
25. Geisler, S., Holmström, K.M., Skujat, D., Fiesel, F.C., Rothfuss, O.C., Kahle, P.J. and Springer, W. (2010) PINK1/Parkin-mediated mitophagy is dependent on VDAC1 and p62/SQSTM1. *Nat. Cell Biol.*, **12**, 119–131.
26. Narendra, D., Tanaka, A., Suen, D.F. and Youle, R.J. (2008) Parkin is recruited selectively to impaired mitochondria and promotes their autophagy. *J. Cell Biol.*, **183**, 795–803.
27. Lee, A.G. (2003) Lipid-protein interactions in biological membranes: a structural perspective. *Biochim. Biophys. Acta*, **1612**, 1–40.
28. Lange, C., Nett, J.H., Trumpower, B.L. and Hunte, C. (2001) Specific roles of protein-phospholipid interactions in the yeast cytochrome bc1 complex structure. *EMBO J.*, **20**, 6591–6600.
29. Hagopian, K., Weber, K.L., Hwee, D.T., Van Eenennaam, A.L., López-Lluch, G., Villalba, J.M., Burón, I., Navas, P., German, J.B., Watkins, S.M. *et al.* (2010) Complex I-associated hydrogen peroxide production is decreased and electron transport chain enzyme activities are altered in n-3 enriched fat-1 mice. *PLoS ONE*, **5**, e12696.
30. Balaban, R.S., Nemoto, S. and Finkel, T. (2005) Mitochondria, oxidants, and aging. *Cell*, **120**, 483–495.
31. St-Pierre, J., Buckingham, J.A., Roebuck, S.J. and Brand, M.D. (2002) Topology of superoxide production from different sites in the mitochondrial electron transport chain. *J. Biol. Chem.*, **277**, 44784–44790.
32. Osaki, Y., Nishino, I., Murakami, N., Matsubayashi, K., Tsuda, K., Yokoyama, Y.I., Morita, M., Onishi, S., Goto, Y.I. and Nonaka, I. (1998) Mitochondrial abnormalities in selenium-deficient myopathy. *Muscle Nerve*, **21**, 637–639.
33. Hill, K.E., Motley, A.K., Li, X., May, J.M. and Burk, R.F. (2001) Combined selenium and vitamin E deficiency causes fatal myopathy in guinea pigs. *J. Nutr.*, **131**, 1798–1802.
34. Rederstorff, M., Krol, A. and Lescure, A. (2006) Understanding the importance of selenium and selenoproteins in muscle function. *Cell Mol. Life Sci.*, **63**, 52–59.
35. Martensson, J. and Meister, A. (1989) Mitochondrial damage in muscle occurs after marked depletion of glutathione and is prevented by giving glutathione monoester. *Proc. Natl Acad. Sci. USA*, **86**, 471–475.
36. Choksi, K.B., Boylston, W.H., Rabek, J.P., Widger, W.R. and Papaconstantinou, J. (2004) Oxidatively damaged proteins of heart mitochondrial electron transport complexes. *Biochim. Biophys. Acta*, **1688**, 95–101.
37. Kim, I., Rodriguez-Enriquez, S. and Lemasters, J. (2007) Selective degradation of mitochondria by mitophagy. *Arch. Biochem. Biophys.*, **462**, 245–253.
38. Tatsuta, T. and Langer, T. (2008) Quality control of mitochondria: protection against neurodegeneration and ageing. *EMBO J.*, **27**, 306–314.
39. Ding, W.X., Ni, H.M., Li, M., Liao, Y., Chen, X., Stolz, D.B., Dorn, G.W. 2nd. and Yin, X.M. (2010) Nix is critical to two distinct phases of mitophagy, reactive oxygen species-mediated autophagy induction and Parkin-ubiquitin-p62-mediated mitochondrial priming. *J. Biol. Chem.*, **285**, 27879–27890.
40. Moraes, C.T., Shanske, S., Tritschler, H.J., Aprille, J.R., Andreetta, F., Bonilla, E., Schon, E.A. and DiMauro, S. (1991) mtDNA depletion with variable tissue expression: a novel genetic abnormality in mitochondrial diseases. Am. J. Hum. Genet., **48**, 492–501.
41. Kim, I. and Lemasters, J.J. (2011) Mitochondrial degradation by autophagy (mitophagy) in GFP-LC3 transgenic hepatocytes during nutrient deprivation. *Am. J. Physiol. Cell Physiol.*, **300**, C308–C317.

サルコメア配列異常を主病変とする筋ジストロフィーの

病因・病態の解明と治療法の開発

Developmental Biology 361 (2012) 79–89

Contents lists available at SciVerse ScienceDirect

Developmental Biology

journal homepage: www.elsevier.com/developmentalbiology

Filamin C plays an essential role in the maintenance of the structural integrity of cardiac and skeletal muscles, revealed by the medaka mutant *zacro*

Misato Fujita [a,1,2], Hiroaki Mitsuhashi [b,1], Sumio Isogai [c], Takahiro Nakata [d], Atsushi Kawakami [a], Ikuya Nonaka [b], Satoru Noguchi [b], Yukiko K. Hayashi [b], Ichizo Nishino [b], Akira Kudo [a,*]

[a] Department of Biological Information, Tokyo Institute of Technology, 4259-B-33 Nagatsuta, Midori-ku, Yokohama 226-8501, Japan
[b] Department of Neuromuscular Research, National Institute of Neuroscience, National Center of Neurology and Psychiatry, 4-1-1 Ogawa-higashi, Kodaira, Tokyo 187-8502, Japan
[c] Department of Anatomy, School of Medicine, Iwate Medical University, 2-1-1 Nishitokuta, Yahaba, Shiwa 028-3694, Japan
[d] Department of Health Science, Ishikawa Prefectural Nursing University, 1-1 Gakuendai, Kahoku, Ishikawa 929-1210, Japan

ARTICLE INFO

Article history:
Received for publication 19 July 2011
Revised 5 October 2011
Accepted 6 October 2011
Available online 14 October 2011

Keywords:
Medaka mutant
Filamin C
Cardiac muscle
Skeletal muscle
zacro

ABSTRACT

Filamin C is an actin-crosslinking protein that is specifically expressed in cardiac and skeletal muscles. Although mutations in the filamin C gene cause human myopathy with cardiac involvement, the function of filamin C *in vivo* is not yet fully understood. Here we report a medaka mutant, *zacro* (*zac*), that displayed an enlarged heart, caused by rupture of the myocardiac wall, and progressive skeletal muscle degeneration in late embryonic stages. We identified *zac* to be a homozygous nonsense mutation in the *filamin C* (*flnc*) gene. The medaka filamin C protein was found to be localized at myotendinous junctions, sarcolemma, and Z-disks in skeletal muscle, and at intercalated disks in the heart. *zac* embryos showed prominent myofibrillar degeneration at myotendinous junctions, detachment of myofibrils from sarcolemma and intercalated disks, and focal Z-disk destruction. Importantly, the expression of γ-actin, which we observed to have a strong subcellular localization at myotendinous junctions, was specifically reduced in *zac* mutant myotomes. Inhibition of muscle contraction by anesthesia alleviated muscle degeneration in the *zac* mutant. These results suggest that filamin C plays an indispensable role in the maintenance of the structural integrity of cardiac and skeletal muscles for support against mechanical stress.

Introduction

Skeletal muscle and heart are the organs that produce physical force by muscle contraction, and muscle fibers are incessantly exposed to strong mechanical stress. To protect intracellular structures against such mechanical stress, muscle fibers express a variety of muscle-specific proteins that often form large complexes.

Two major protein complexes, the dystrophin-associated glycoprotein complex (DGC) and the integrin complex are known to have important roles in affording mechanical integrity to striated muscle. In skeletal muscle, these complexes, which are localized at the sarcolemma (Arahata et al., 1988; Mayer, 2003; Watkins et al., 1988) and myotendinous junctions (MTJs; (Bao et al., 1993; Samitt and Bonilla, 1990; Shimizu et al., 1989), where the muscle fibers are connected to tendon, link the subsarcolemmal actin cytoskeleton to the extracellular matrix (ECM) (Burkin and Kaufman, 1999; Campbell, 1995; Yoshida et al., 2000). Defects in the components of this DGC lead to muscular dystrophy (Bonnemann et al., 1995; Hoffman et al., 1987; Lim et al., 1995; Nigro et al., 1996; Noguchi et al., 1995; Roberds et al., 1994), an inherited muscular disorder characterized by progressive muscle degeneration, suggesting the importance of this linkage system for the integrity of muscle fibers. Muscle fibers specifically express α7β1 integrin, and a defect of α7 integrin causes muscular dystrophy, primarily affecting muscle fibers close to the MTJs (Hayashi et al., 1998; Mayer et al., 1997; Miosge et al., 1999), pointing to the importance of the integrin-based linkage for muscle integrity, particularly at MTJs. In heart, DGC and integrins are localized at the sarcolemma as well as at intercalated disks, which are the contact sites between cardiomyocytes (Anastasi et al., 2009; van der Flier et al., 1997).

The Z-disk is a huge multi-protein complex that constitutes the border of individual sarcomeres. This Z-disk plays a key role in the crosslinking of actin thin filaments of myofibrils to withstand the extreme mechanical force generated during muscle contraction. Z-disks are attached to the sarcolemmal DGC and integrin complexes at the sites of costameres via Z-disk-associated linker molecules (Ervasti, 2003). Recently, mutations in genes encoding Z-disk components have been found to be responsible for a group of muscle diseases termed myofibrillar myopathy, which is pathologically characterized by myofibrillar disorganization, including the degeneration of the

* Corresponding author. Fax: +81 45 924 5718.
E-mail address: akudo@bio.titech.ac.jp (A. Kudo).
[1] Misato Fujita and Hiroaki Mitsuhashi were equal contributors to this study.
[2] Present address. Section on Vertebrate Organogenesis, Program in Genomics of Differentiation, Eunice Kennedy Shriver National Institute of Child Health and Human Development, National Institutes of Health, MD 20892, USA.

0012-1606/$ – see front matter © 2011 Elsevier Inc. All rights reserved.
doi:10.1016/j.ydbio.2011.10.008

sarcomere structure (Selcen, 2008; Selcen et al., 2004). These reports suggest that Z-disk proteins have important roles in maintaining organized sarcomere structures.

Filamins are actin-crosslinking proteins first purified by their ability to bind and precipitate actin (Hartwig and Stossel, 1975; Stossel and Hartwig, 1975). Filamins are composed of 3 isoforms, filamins A, B, and C. All filamins consist of an N-terminal actin-binding domain followed by 24 immunoglobulin-like repeats, and they dimerize at the 24th repeat domain located at the C-terminus (Stossel et al., 2001). Filamins directly interact with more than 30 diverse proteins, and are involved in multiple cellular processes including cell–cell and cell–matrix adhesion, mechanoprotection, actin remodeling, and various intracellular signaling pathways (Feng and Walsh, 2004). Filamin C is a muscle-specific isoform and localizes at MTJs, costameres, Z-disks, and intercalated disks in mammal and avian muscles (Ohashi et al., 2005; van der Ven et al., 2000a). Interestingly, filamin C interacts with both DGC (Thompson et al., 2000) and integrin (Gontier et al., 2005; Loo et al., 1998), as well as with the Z-disk proteins myotilin (van der Ven et al., 2000b), FATZ-1 (Faulkner et al., 2000), and myopodin (Linnemann et al., 2010) through its C-terminal region. Such localization and protein interaction suggest that filamin C functions in maintaining the mechanical integrity of muscle cells. Recently, mutations in the filamin C gene were identified in patients having myofibrillar myopathy (Kley et al., 2007; Luan et al., 2010; Shatunov et al., 2009; Vorgerd et al., 2005). These patients frequently develop cardiac abnormalities in addition to skeletal myopathy, suggesting the essential role of filamin C in both skeletal and cardiac muscles. To investigate the function of filamin C *in vivo*, Dalkilic et al. (2006) generated *filamin C*-deficient mice having a deletion of the last 8 exons of *Flnc*. This deficient mouse shows fewer muscle fibers or primary myotubes than normal and abnormal rounded fibers, suggesting defects in primary myogenesis; however, this mouse does not present any cardiac defects, which indicates a partial-loss-of-function. Since these mice die *in utero* or live only a short while after birth, further detailed observations cannot be carried out.

Recently, zebrafish have emerged as an alternative model organism to study the vertebrate muscular system and to isolate new dystrophy-causing genes/pathways (Guyon et al., 2007; Steffen et al., 2007). A deficiency of DGC or integrin-linked kinase causes a muscular dystrophic phenotype in zebrafish embryos (Bassett et al., 2003; Cheng et al., 2006; Gupta et al., 2011; Guyon et al., 2005; Postel et al., 2008), suggesting that their functions are likely to be analogous to those in humans. In zebrafish embryos, the DGC is localized initially at the junctional area, where the ends of muscle fibers attach to the myosepta, corresponding to the myotendinous junction (MTJ). Loss of DGC causes muscle fiber detachment at MTJs, indicating compromised adhesion between muscle fibers and the ECM of myosepta. Medaka (*Oryzias latipes*), another teleost fish, has the experimental advantages of external development, transparency, and quick production of a number of embryos, similar to the zebrafish. Unlike zebrafish, however, various medaka inbred strains have been established; and the medaka genome, which is about one-half of the size of the zebrafish genome, is almost fully sequenced and aligned, indicating that the medaka has powerful advantages for the application of forward genetics (Ishikawa, 2000; Wittbrodt et al., 2002).

Here, we identified a medaka mutant, *zacro* (*zac*), that has a nonsense mutation, resulting in an early truncation at the 15th immunoglobulin-like repeat of the medaka orthologue of filamin C. This mutation causes myocardiac rupture in the ventricle. Although this mutant displayed normal myogenesis in myotome muscles during early stages of embryonic development, its myofibrils gradually degenerated and became disorganized in later stages. Detailed histological analysis suggests an indispensable role of filamin C in the maintenance of the muscle structure rather than in its formation in both heart and skeletal muscles.

Materials and methods

Medaka strains and mutant screening

All studies requiring wild-type medaka (*O. latipes*) were carried out by using the Qurt strain, which was derived from the southern population (Wada et al., 1998). Fish were maintained in an aquarium system with re-circulating water at 28.5 °C. Embryos were obtained from natural spawning, and incubated at 28 ± 2 °C. Stages were determined as previously described (Iwamatsu, 2004). *N*-ethyl-*N*-nitrosourea (ENU) was used for mutagenesis, and a standard genetic F3 screening for mutations affecting embryogenesis were performed as described earlier (Ishikawa, 1996; Ishikawa et al., 1999). The *zac* mutant was identified by microscopic inspection as a Mendelian-inherited recessive lethal mutation that caused a phenotype characterized by congestion in the blood vessels and pericardial edema.

Positional cloning

zac heterozygous fish, which were maintained on the southern Qurt genomic background, were mated with the northern HNI strain fish (Hyodo-Taguchi, 1980) to generate F1 families. Embryos for the genetic mapping were obtained from inter-crosses of F1 *zac* carriers. To locate the genetic linkage, we conducted bulk segregant analysis on pools of genomic DNA from *zac* mutants and wild-type embryos by using sequence tagged site (STS) markers on the medaka genome (Kimura et al., 2004). The *zac* region was narrowed down by using additional STS markers, AU171271 and Olb2110h (Naruse et al., 2000), and newly designed restriction fragment length polymorphism (RFLP) markers, HAL and KCND2 (HAL; 5′-GGATGGGCAGATGCCAAATATG-3′ and 5′-GTCCCGTTGATCAGAGCCAG-3′/MboI, KCND2; 5′-CAGCAGGTGTAGCGGCATG-3′ and 5′-GTTGGCCATCACTGATATGGC-3′/AfaI). cDNAs of *flnc* from *zac* mutant and wild-type embryos were amplified, and verified by sequencing. The full-length cDNA of *flnc* was cloned by PCR using primers including XbaI restriction enzyme sites [5′-CAATCTAGACAAGGAACAAGCC-3′ and 5′-GAATCTAGACCACCATTTAGCC-3′], and was sequenced. We obtained 2 different *flnc* clones, which appeared to be splice variants. To confirm the linkage between the *zac* mutation and *flnc* gene, we performed allele-specific PCR using 2 independent outer primers [5′-TTCAGTTGGAGGACATGGGAT-3′ and 5′-GACACCTGCAACACAACTCTA-3′] in combination with either a wild type-specific antisense primer [5′-CTTGCAGGTCACCTTTCCTTT-3′] or a mutant-specific one [5′-CTTGCAGGTCACCTTTCCTTA-3′]. We also performed 5′-RACE and 3′-RACE to obtain full-length sequence information on *flnc* cDNA. The sequences of the medaka *flnc* have been deposited in GenBank under the accession numbers AB639344 and AB639345.

Birefringence assay

Embryos were dechorionated at stage 27. Muscle birefringence was analyzed at stages 32 and 34 by placing anesthetized embryos on a glass dish and observing them with an underlit dissecting scope (Olympus, SZX12) having 2 polarizing filters (Olympus, SZX-P0 and SZX2-AN). The top polarizing filter was twisted until only the light refracting through the striated muscle was visible.

Histological analysis

Embryos were fixed overnight at 4 °C in 4% paraformaldehyde (PFA) in phosphate-buffered saline pH 7.4 (PBS), dehydrated by ethanol, and embedded in a resin (Technovit 8100, Kulzer Heraeus) according to the manufacturer's instructions. Sections were cut at 2 μm and stained with Harris's hematoxylin and Eosin Y or Masson trichrome staining buffer (SIGMA).

Whole-mount RNA in situ hybridization

Whole-mount RNA *in situ* hybridization was performed as previously described (Inohaya et al., 1995; Inohaya et al., 1999). Digoxigenin-labeled antisense RNA probes for cardiac myosin light chain 2 (*cmlc2*), desmin (*des*), *flnc*, *myf5*, *nkx2.5*, *tbx5a*, and ventricular myosin heavy chain (*vmhc*) were used. The primer sets used for cloning the respective probes are listed below.

cmlc2 F: AATGTCTTTTCCATGTTYGARC
R: CAGATTCAGCAGTTTAARGARG and CTCCTCTTTCTCATCHCCATG
des F: AACAACCAGCCAACCATGAGC
R: ACAGATGTAGTTATCCTGCAGG
flnc F: GCTCCAGAGGAAATTGTGGAC
R: CTCACACCTTTAGGCTGTAGC
myf5 F: ATCCACTTCTTCTCCCCAGC
R: TTTCTCCTCAGAGAGAACCG
*nkx2.5*F: TTCTCTCAGGCGCAGGTGTACGAGC
R: GCDGGGTAGGYGTTGTA
tbx5a F: GTCTGAGATTTTCCGAGCTCC
R: CTCTCTCTAGACTCGAGTTGGTCCTTCTTGTGTTCTCCC
vmhc F: GGAGCTGGATGATGTGGTTTC
R: CATGGGCTAAGGCGTTCTTGGC
(R: A,G. Y: C,T. H: A,C,T)

Injection of morpholino antisense oligonucleotide (MO)

We obtained a specific MO (Gene Tools) to interfere with *flnc* translation. The MO [5′-GGCCATCATGTTGGCTTGTTCCTTG-3′] was dissolved at concentrations from 100 to 1000 μM in nuclease-free water. Approximately 0.5 nl of MO solution or standard control MO [5′-CCTCTTACCTCAGTTACAATTTATA-3′] was injected into 1-cell-stage embryos.

Whole-mount immunofluorescence

Dechorionated embryos were anesthetized in 0.02% tricaine methanesulfonate and fixed in 4% PFA in PBS at 4 °C overnight. We used chilled methanol at −20 °C as the fixative for anti-laminin antibody, and IHC Zinc fixative (BD Biosciences) for anti-γ-actin antibody. After fixation, embryos were dehydrated in a graded series of methanols (25–50–75%) and stored in 100% methanol at −20 °C. Embryos were rehydrated in a graded series of methanols (75–50–25%) and washed 3 times for 15 min each time in MABTr (0.1 M maleic acid and 150 mM NaCl containing 0.1% Triton X-100) and subsequently in MABDTr (MABTr with 1% BSA and 1% DMSO) twice for 30 min each time. Following blocking with 5% goat serum in MABDTr for 30 min, the embryos were incubated with primary antibodies at 4 °C overnight. The following antibodies were used: anti-filamin C (SIGMA HPA006135; 1:100), anti-vinculin (SIGMA V4505; 1:50), anti-α-actinin (SIGMA A7811; 1:500), anti-integrin β1D (Millipore MAB1900; 1:25), anti-β-sarcoglycan (Novocastra NCL-b-SARC; 1:50), anti-slow muscle myosin heavy chain (F59, DSHB; 1:100), anti-FAK pY397 (Invitrogen 44-625G; 1:100), anti-dystrophin (SIGMA D8043; 1:100), anti-β-dystroglycan (Novocastra NCL-b-DG; 1:100), and anti-phospho-paxillin (Cell Signaling Technology #2541; 1:50). Rabbit polyclonal anti-cytoplasmic γ-actin antibody was previously characterized (Nakata et al., 2001), and used at a dilution of 1:100. Embryos were washed 6 times in MABDTr for 15 min each time, and then incubated with Alexa488-conjugated anti-rabbit IgG or Alexa568-conjugated anti-mouse IgG (Molecular Probe; 1:800) at 4 °C overnight. Primary and secondary antibodies were diluted in Can Get Signal immunostain solution A (TOYOBO). After 6 more washings in MABTr, the embryos were whole-mounted on glass slides and observed with a confocal microscope (LSM 700, Zeiss).

Electron microscopy

For observation using transmission electron microscope (TEM), embryos were dechorionated and fixed at stage 27, 29, 30, 32 or 36 in 100 mM cacodylate buffer (pH 7.4) containing 2% glutaraldehyde and 4% PFA at 4 °C overnight. Samples were post-fixed in 0.06 M s-collidine buffer (pH 7.2) containing 1.3% osmium tetroxide and 0.5% lanthanum nitrate, dehydrated by passage through a graded series of ethanols, and finally embedded in Epon 812 (Taab). Longitudinal sections (120 nm) were stained with 3% uranyl acetate for 20 min and then with 0.4% lead citrate for 5 min. Sections were viewed with a Tecnai Spirit transmission electron microscope (FEI) or a Hitachi H-7100 or H-7650 electron microscope (Hitachi).

For observation using scanning electron microscopy (SEM), embryos were fixed in 0.1 M phosphate buffer (PB, pH 7.4) containing 2.5% glutaraldehyde and 2% PFA. The yolk were removed from the embryo with forceps to expose the heart, and postfixed for 2 h in 1% osmium tetroxide in PB at 4 °C. The embryos were then rinsed in PB, dehydrated in a graded series of ethanol, frozen in t-butyl alcohol, then freeze-dried *in vacuo* with an Eiko ID-2. The embryos were mounted on a metal stub, osmium-coated by using a Filgen OPC60A, and observed with an HS-6 electron microscope (Hitachi).

Muscle relaxation assay

Embryos were incubated with anesthetized in 0.0015% tricaine methanesulfonate in embryo medium for 48 h from stages 27 to 32 to prevent muscle contractions. Treated and untreated embryos were immunostained with F59 antibody obtained from the Developmental Studies Hybridoma Bank at stage 32, and the number of somites with muscle-fiber degeneration was counted.

Results

Enlarged ventricle and muscle disorganization in zac mutants

zacro (*zac*) is a recessive, embryonic-lethal mutant obtained by ENU (*N*-ethyl-*N*-nitrosourea) mutagenesis. *zac* mutants were characterized by an abnormally enlarged heart with a gradually reduced blood flow. The normal medaka heart starts to beat at stage 24, and blood flow begins at stage 25. No difference was observed until stage 25 in *zac* embryos; however, by stage 28 prior to the heart looping, *zac* mutants showed blood congestion in the ventricle along with pericardial edema (Figs. 1A, B). Ruptures in the myocardium layer were detected in the *zac* mutants at stage 27, especially in the dorsal-right myocardium of the ventricle (Figs. 1C, D asterisk). As the endocardium was intact in *zac* mutants, we speculate that the blood accumulation was caused by ineffective contraction of the torn myocardium. *zac* mutants appeared to be normal in their somite differentiation during the early stages of somitogenesis; however, by stage 32, they frequently exhibited an abnormal curvature with their tails dorsally up instead of having the normal flat body axis (Figs. 1E, F). We further analyzed the birefringence of myotome muscle of *zac* mutants by using polarized filter microscopy. Birefringency is used to assess muscle organization in zebrafish models of muscle disease (Granato et al., 1996). Wild-type embryos from stage 32 onwards displayed high birefringence due to the ordered array of their myofilaments (Figs. 1G, I), whereas *zac* mutants displayed patchy birefringence at this stage (Fig. 1H), indicating muscle disorganization in some somites. Muscle disorganization in the *zac* mutant continued to progress, and most of the somites lost their birefringence by stage 34 (Fig. 1J). Histological analysis revealed that orientation of each myotube was severely disorganized by stage 40 (Figs. 1K, L).